INFORMATION TO USERS

This material was produced from a microfilm copy of the original document. While the most advanced technological means to photograph and reproduce this document have been used, the quality is heavily dependent upon the quality of the original submitted.

The following explanation of techniques is provided to help you understand markings or patterns which may appear on this reproduction.

1. The sign or "target" for pages apparently lacking from the document photographed is "Missing Page(s)". If it was possible to obtain the missing page(s) or section, they are spliced into the film along with adjacent pages. This may have necessitated cutting thru an image and duplicating adjacent pages to insure you complete continuity.

2. When an image on the film is obliterated with a large round black mark, it is an indication that the photographer suspected that the copy may have moved during exposure and thus cause a blurred image. You will find a good image of the page in the adjacent frame.

3. When a map, drawing or chart, etc., was part of the material being photographed the photographer followed a definite method in "sectioning" the material. It is customary to begin photoing at the upper left hand corner of a large sheet and to continue photoing from left to right in equal sections with a small overlap. If necessary, sectioning is continued again — beginning below the first row and continuing on until complete.

4. The majority of users indicate that the textual content is of greatest value, however, a somewhat higher quality reproduction could be made from "photographs" if essential to the understanding of the dissertation. Silver prints of "photographs" may be ordered at additional charge by writing the Order Department, giving the catalog number, title, author and specific pages you wish reproduced.

5. PLEASE NOTE: Some pages may have indistinct print. Filmed as received.

University Microfilms International
300 North Zeeb Road
Ann Arbor, Michigan 48106 USA
St. John's Road, Tyler's Green
High Wycombe, Bucks, England HP10 8HR

A TECHNIQUE TO PERFORM PRECISION DAYTIME ASTROMETRY

by

Alfred Webb Healy

A Dissertation Submitted to the Faculty of the

DEPARTMENT OF PHYSICS

In Partial Fulfillment of the Requirements
For the Degree of

DOCTOR OF PHILOSOPHY

In the Graduate College

THE UNIVERSITY OF ARIZONA

... 1 9 7 7

THE UNIVERSITY OF ARIZONA

GRADUATE COLLEGE

I hereby recommend that this dissertation prepared under my direction by Alfred Webb Healy

entitled A Technique to Perform Precision Daytime Astrometry

be accepted as fulfilling the dissertation requirement for the degree of Doctor of Philosophy

Henry Allen Weis — Dissertation Director

4-20-77 — Date

As members of the Final Examination Committee, we certify that we have read this dissertation and agree that it may be presented for final defense.

Troy Bletzer	22 April 1977
R. H. Tannenbaum	20 April 1977
K. C. Hsieh	20 April 1977
J. J. Vuillemin	20 April 1977

Final approval and acceptance of this dissertation is contingent on the candidate's adequate performance and defense thereof at the final oral examination.

STATEMENT BY AUTHOR

This dissertation has been submitted in partial fulfillment of requirements for an advanced degree at The University of Arizona and is deposited in the University Library to be made available to borrowers under rules of the Library.

Brief quotations from this dissertation are allowable without special permission, provided that accurate acknowledgment of source is made. Requests for permission for extended quotation from or reproduction of this manuscript in whole or in part may be granted by the head of the major department or the Dean of the Graduate College when in his judgment the proposed use of the material is in the interests of scholarship. In all other instances, however, permission must be obtained from the author.

SIGNED: Alfred W Healy

ACKNOWLEDGMENTS

The author gratefully acknowledges the invaluable assistance of Professor Henry A. Hill for his guidance in the preparation of this dissertation.

Many other people furnished aid, encouragement, education and friendship in the course of my graduate education. Drs. Paul Clayton, James Oleson, Douglas Patz, Robin Stebbins, and Carl Zanoni, as well as Paul Ballard and Francisco Smolka, deserve special mention for their contributions, too numerous to cite individually.

This work was supported by the National Science Foundation, The University of Arizona, and Wesleyan University.

The author is especially grateful for an understanding wife whose support has been invaluable during this undertaking.

Finally, Barbara Bickel is thanked for her preparation of this document while the author was in absentia.

TABLE OF CONTENTS

TABLE OF CONTENTS--Continued

LIST OF ILLUSTRATIONS

LIST OF TABLES

ABSTRACT

Several questions of importance to the physics and astronomy communities can be answered with data furnished by a regime of precision daytime astrometry. A radical departure from previous astrometric instruments has led to the development of an instrument with an ultimate design accuracy of 0.001 arc seconds.

The Schupmann medial telescope optical design is exploited to give a low scattering device which compensates for its own chromatic aberrations and the lateral chromatic aberration of the atmosphere. The solution to the problem of star detection in the presence of a bright nonuniform sky background is discussed.

The essential features of star tracking are demonstrated by tracking Polaris through sunrise with the instrument.

CHAPTER 1

INTRODUCTION TO PRECISION DAYTIME ASTROMETRY

Astrometry is that area of astronomy which deals with the measurement of the positions and motion of celestial objects. Although not defined as such, astrometry has existed since about 3000 B.C. At this early date, Mesopotamian astronomers recorded the precession of the vernal equinox by noting that the signs of their zodiac were gradually shifting westward with respect to the corresponding constellations.

Historically each generation has tried to perfect its astrometric technology in order to answer questions posed by the previous generation. This dissertation details a technique to make astrometric measurement more precise than previously possible. In so doing, data accurate enough to answer certain specific questions can be provided. The level of precision that can be achieved and what scientific information can be gained at that level of accuracy will be discussed.

An important branch of astrometry is devoted to the measurement of the position of objects which appear near the Sun. The overwhelming daytime sky brightness to object brightness ratio makes these measurements exceedingly difficult. There are however, problems in physics and astronomy which can be answered most directly by daytime astrometry. Observing a star as it appears to pass behind the Sun affords the opportunity to test General Relativity via the gravitational deflection of

starlight. Observing several stars establishes the Earth's orbit with respect to the fixed stars. Coordinating the time of observations to an atomic clock yields a measurement of the time rate of change in the gravitational "constant" with respect to atomic time.

Current daytime astrometry techniques are of two types: (1) eclipse photographs and (2) microwave frequency measurements. Eclipse photographs have been taken for more than the past fifty years. However, there have only been 40 eclipses [1] in this period, and many have been unsuitable because of inaccessibility or poor weather conditions.

The ultimate accuracy of eclipse measurements is limited by the severe field conditions imposed. An individual eclipse measurement yields an accuracy of about 0.1 arc second. The rarity of events and expense per datum make this an awkward method of pursuing astrometric problems.

Nonoptical wavelength measurements have been of the long baseline radio-interferometry type. These yield little in absolute position measurements but have been used in gravitational deflection measurements with success [2]. There are relatively few objects in the heavens to use for deflection measurements. The overall accuracy of the radio-interferometry method is about 0.002 arc second under best conditions. The technique of measuring the differential deflection of two close sources is used. This differential is about 0.2 arc second. Thus, an accuracy of 0.002 arc second represents a 1% determination in the gravitational deflection of light.

The Santa Catalina Laboratory for Experimental Relativity by Astrometry (SCLERA) instrument has an overall design accuracy of 0.001 arc second (SCLERA is a research facility jointly operated by The University of Arizona and Wesleyan University). The time of data acquisition can by synchronized to the National Bureau of Standards (NBS) time standards for obtaining equally accurate position versus time measurements. The observation time is limited only by the requirement of having the Sun and the star or planet about 30 degrees above the horizon. Thus, an object can be tracked for a sufficiently long period of time to greatly reduce statistical errors.

A primary function of the telescope is to measure the gravitational deflection of light. Here, the ultimate accuracy of the SCLERA instrument represents one to two orders of magnitude improvement over existing optical measurement and possibly an order of magnitude improvement over radio astronomy techniques.

The gravitational deflection of starlight at the solar limb is 1.7 arc seconds. At the closest point to the limb at which a star may be tracked, the deflection is about 1 arc second. Hence the instrumental design accuracy of 0.001 arc second results in a 0.1% measurement of this quantity. This compares very favorably to the 1% measurements of equivalent quantities by radio astronomy techniques. Additionally, data can be simultaneously obtained on other important phenomena. Since the telescope was designed to incorporate an atomic time standard through a WWVB (60 kHz) rado link to NBS, instantaneous right ascension and declination could be obtained. A comparison of astronomical and

atomic time would be a direct result of measuring the apparent motion of the Sun as a function of atomic time. An observing regime which spanned ten years would provide relevant information on possible changes in the universal gravitational constant.

The precession of the perihelion of the Earth's orbit could be determined to sufficient accuracy to provide additional observational data on the relativistic precession of planetary orbits. Currently, solar oblateness measurements are used to determine the visual oblateness of the Sun and a mass quadrupole moment is deduced from that oblateness. The quadrupole moment of the Sun gives rise to classical perihelion advance with a different radial dependence than the relativistic term. Knowing the perihelion advance of two planets sufficiently accurately allows a determination of the relativistic perihelion advance free of any uncertainty in how the visual solar oblateness is related to its mass quadrupole moment.

Tracking Mercury at superior conjunction would improve our knowledge of the perihelion advance of the planet and hence allow a better comparison between the predictions of General Relativity and observed data.

The coordinates of the plane of the Earth's orbit could be more accurately established with respect to the celestial sphere. At present this is known to only 0.02 arc second [3].

The techniques of daytime astrometry could easily be used for nighttime astrometry with no loss of accuracy. Parallax measurements of 0.001 arc second accuracy would be of great benefit to astronomy by

providing trigonometric distances to more distant stars and stars of varied spectral types. Stars of known parallax are the only means of calibrating the absolute luminosities and bolometric corrections of stars. More accurate proper motion of stars would result in a more accurate determination of the dynamics of star clusters, velocity dispersions as a function of spectral type, and galactic rotation. The anomalous behavior of such objects as Barnard's Star [3] could be more accurately observed and possibly help clarify the phenomenon.

Progress in astrometry can be achieved in two ways. The first is to refine existing techniques, e.g., more stable photographic plates. The second is to develop new techniques and adapt new technologies. The second approach has been used in the design of the SCLERA telescope, because the problems at the desired accuracy levels seem to be insurmountable with existent astrometric techniques and technologies.

The basic design of the SCLERA telescope is discussed by Oleson et al. [4]. The most important features will be discussed here. The image of a star observed through the atmosphere has a small random motion due to varying atmospheric refraction. This phenomenon is called seeing. Gross seeing is the random motion of a portion of the sky as a unit. Gross seeing and systematic effects such as refraction are reduced by servoing the Sun's image to a finely defined position by a primary tracker. Stars near the Sun have the same zeroeth order systematic effects in position as the Sun; hence, relative measurements would be free of this systematic error. The SCLERA instrument uses the position of the Sun as the center of a coordinate system. The Sun's

diameter is taken to be a constant and measured fluctuations in the solar diameter are interpreted as scale changes in the coordinate system. This removes much of the systematic effect of changes in telescope parameters and first order atmospheric effects.

Lateral chromatic aberration produced by the dispersion of the atmosphere and longitudinal chromatic aberrations of the objective are reduced by a factor of 100 over a selected bandwidth by the use of a Mangin system [5]. Chronograph quality achromatic doublets are beyond the state of the art with respect to scattering and multiple scattered images. Hence a singlet must be used for daytime astrometry. Doublets depend on the cancellation of large but opposite signed aberrations to achieve a usable lens. The residual aberrations of such a lens render them unusable in a system with the design accuracy of SCLERA. The longitudinal chromatic aberration of the objective amounts to about 60 cm over the effective bandwidth of 300 nm. This is reduced to less than the depth of focus of the objective by the Mangin system. Lateral chromatic aberration of the atmosphere for a 4000-7000Å bandwidth at an elevation of 2600 meters (8500 feet) amounts to about 1.0 arc second for a zenith angle of 45°. This is reduced to 0.01 arc second optically and the remaining aberration is handled by modeling the effect by a known function of site atmospheric parameters and zenith angle (cf. Chapter 4). Again, an improve signal-to-noise ratio is the result of the wideband detection methods allowed by the removal of both atmospheric and instrumental chromatic aberration.

Apodization of the objective by a square stop with the diagonal along the star-Sun direction reduces diffraction into the field of the star detector by a factor of 10^4 [6].

Stars appear to move about 0.04 arc seconds/sec with respect to the Sun. Much important information is contained in a star position measurement as an accurate function of time. Previous measurements have been of two types, eclipse photographs [7] and meridian circle measurements [3]. Both methods are subject to systematic errors, the magnitudes of which are difficult to estimate. Eclipse photographs are necessarily taken under field conditions and lack the option of repetitive measurements. Meridian circle measurements rely on the observers judgment as to when a star image crosses a line. Hence a personal judgment enters into the data taking process. The design employed at SCLERA uses a photoelectric phase sensitive detection system to track a star. The diameter of the Sun is measured using a finite Fourier transform definition [8] technique to determine its edge. The distance between the two edges of the Sun as well as the distance from the near edge of the Sun to the star being tracked is measured interferometrically.

CHAPTER 2

IMPORTANCE OF PRECISION DAYTIME ASTROMETRY AND CURRENT TECHNIQUES

A program of precision astrometry can make significant contributions to the areas of gravitational phenomena, cosmology, and parallax studies, and more accurately determine the orbit of the Earth. These points are discussed in the following sections.

Tests of General Relativity

Since its inception, Einstein's theory of General Relativity has been the most widely accepted description of gravitational phenomena. It's early success in predicting the precession of the perihelion of Mercury and its uncontrived appearance established this theory's preeminence. Yet elegance is not proof. No theory with such far reaching consequences has such a small amount of proof as does General Relativity. Experiments which can give additional verification or perhaps disprove General Relativity are desparately needed. In the intervening six decades since Einstein's "Three Tests" were proposed, great advances in technology have been made. Newer methods have been proposed to perform the original experiments and additional tests have been postulated. These tests can be divided into two broad classes, gravitational deflection of light and relativistic orbital perturbations. Each of these classes will be discussed in detail.

The gravitational deflection of light and its variations comprise a number of experimental tests of General Relativity. Three approaches have been taken to the problem: (1) radar ranging of planets and artificial satellites as they pass behind the Sun, (2) radio interferometric techniques using distant microwave sources, e.g., radio galaxies, and (3) optical measurements of the star's position as it appears to pass behind the Sun. In each case, the Sun is used as the gravitational source. There are difficulties associated with each of these experiments.

The corona, being a plasma with a radial density gradient, is the dominating source of difficulty in the first two cases [9]. The sky brightness and the radial brightness gradient are the dominant difficulties associated with the third case.

Jupiter has no plasma corona surrounding it nor does it have a brightening effect on the local sky. For these reasons it might be thought that Jupiter would be a suitable object for gravitational deflection measurements. The limb deflection of starlight for the Sun is 1.75 arc seconds, that of Jupiter is about a factor 10^2 less. Consequently, a 1% measurement, for instance, requires an accuracy of 1.75×10^{-4} arc second if Jupiter is used. The technical problems at the tenth's of milliarc seconds level make Jupiter an unfavorable choice.

Radar Ranging Techniques and Results

Radar ranging of planets and artificial satellites offers positional and velocity information. This information can be used in a test of General Relativity. Doppler velocity measurements [10] have errors

of several parts in 10^6 while time of flight measurements [10] have errors of about one part in 10^8. Because of their inherent higher accuracy the time of flight measurement's contribution to the understanding of General Relativistic phenomena will be considered first.

Calculations of Shapiro [10] show that for radar waves passing near the Sun, a 200 μsec relativistic delay in round trip time of flight from Earth to a planet at superior conjunction will be observed. In particular a delay $\Delta\tau_r$ is found to be [10]

$$\Delta\tau_r = \frac{4GM_s}{c}\left\{\ell n\left[\frac{x_e+r_e}{x_p+r_p}\right] - \left[\frac{x_e-x_p}{r_e}\right]\right\} \qquad (1)$$

where M_s is the mass of the Sun, x_e and x_p are the radar path lengths from the Earth and planet to the point of closest approach to the Sun on the path of the radar wave, and r_e and r_p are the distances from the Sun to the Earth and planet respectively. Figure 1 gives a plot of $\Delta\tau_r$ as a function of a planet's angular distance from the Sun.

The most usable information comes from the time delay at superior conjunction. Here a 1% measurement requires errors to be 2 μsec or smaller. The planetary surfaces must be resolved to 300 m and solar coronal plasma effects must be known to commensurate accuracies. The planetary surface resolution problem may be resolved by determining a "signature" of the reflected radar beam which is the integrated reflectivity of all the planet's structure. Rotational properties of the planet could be incorporated into the signature by determining a periodic signature. Correlation of signatures of different phases would

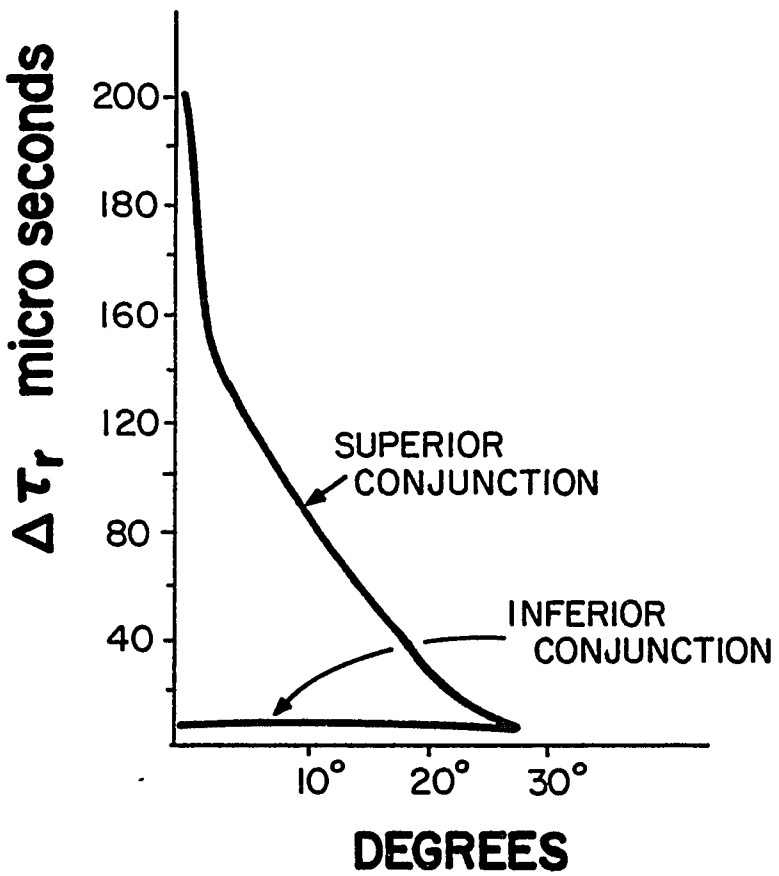

Figure 1. Relativistic radar time of flight increase versus angular separation of Sun and Mercury.

Taken from Shapiro [10].

remain a problem which could be resolved by observing a planet when the change in the relativistic propagation decay is minimal. Nonperiodic fluctuations would still pose a problem. Variations due to atmospheric phenomena or seasonal reflectivity changes would not be amenable to signature techniques. The reflection signature technique has proven to be of some value but has not determined a planetary position criterion to the 300 m accuracy requirement.

Solar corona plasma effects must also be considered in a radar experiment. At 8 GHz, a few nsec change in the time delay is expected at angles less than 1° from the Sun. This is unacceptable for the type of accuracies required. Two possible methods could be used to avoid this problem. Higher frequencies could be used or two frequencies could be used and the plasma term could then be extracted. Higher frequencies have limitations in that existing radar technology must be used. Cost factors in developing new radars prohibit going above what is commercially available in radar transmitters and receivers. Two frequency radar work requires duplicate transmitters and receivers. Since the corona effect varies as the inverse of the square of the radar frequency the corona effect could be removed completely in theory. In practice the problem of simultaneous measurements at two radar frequencies has not been surmounted.

Planetary radar ranging has resulted in measurements equivalent to gravitational starlight deflections with 4-8% uncertainties [11]. Part of the radar ranging problem could be solved if a satellite transponder were used. The complex problem of removing planetary surface

features from the data would be eliminated. Mariner IV had such a transponder. Successful tracking of Mariner IV in March and April of 1966 resulted in the best measurements of their kind. The solar plasma difficulties however limited these measurements to a few percent accuracy [12].

Doppler shift measurements offer little in the way of tests of General Relativity. Colocation of transmitter and receiver in radar ranging of planets precludes the measurement of a gravitational red shift. There is an effect [10], third order in v_p/c, where v_p is planetary velocity relative to radar transmitter, which might be used to test General Relativity. Shapiro [10] calculates this effect to produce a fractional frequency shift in the received signal $\Delta f/f$ of 4×10^{-10} for Venus and 1.2×10^{-9} for Mercury at solar grazing incidence. This is 10^{-10} for 1° Sun-Venus separation. Effects of this magnitude would be detectable only under the most favorable conditions and certainly a 1% measurement is not feasible.

Radio Interferometric Techniques and Results

Long baseline radio interferometric techniques of the last several years have resulted in gravitational deflection of starlight measurements of 1%. Fomalont and Sramek [2] have measured a deflection of 1.775 ± 0.019 arc seconds at the solar limb. Their technique differs from previous measurements in that (1) radio sources were tracked at two frequencies, 2.695 GHz and 8.085 GHz, and (2) three nearly colinear radar sources (0111+02, 0116+08, 0119+11) were tracked rather than the customary two sources. This change in observing technique offers

sufficient data to calculate the plasma effect using well understood models of electromagnetic wave propagation through a plasma. Information on other systematic errors is also collected, allowing correlations to be made for them.

Eclipse Measurements

Optical measurements of the gravitational deflection of starlight have been limited to date to eclipse measurements. Eclipse measurements are hampered by the rarity of the events and severe field conditions. Measurements of 0.70 ± 0.10 arc seconds [7] and 1.43 ± 0.15 arc seconds are typical of these measurements. The observing time is about a minute per year and much of that is not usable because of cloud cover at the observing site. There is no reason to believe the above quoted measurements are without systematic errors. Efforts continue to perform these observations; however, instrumentation is not being developed to improve upon existing measurements.

The SCLERA Instrument

The SCLERA instrument has a design capability of reducing systematic errors to 0.001 arc second. If it is assumed that a star can be tracked to one solar radius from the limb, a measurement of 0.8 ± 0.001 arc second would result. This corresponds to 1.7 ± 0.002 arc seconds at the limb. This represents a 0.1% measurement and a factor of $\sim$ 10 improvement over existing measurements.

A large amount of General Relativistic theory and calculations have been put forth based on an anomalously small amount of experimental

fact. A second 1% measurement of the gravitational deflection of light is certainly needed in such a case. A 0.1% measurement of starlight deflection could possibly reveal higher order corrections to the theory if they are present.

The perihelion advance of the planet Mercury was first cited as the conclusive proof of General Relativity. A 43.11 ± 0.45 arc seconds per century residual (after all known classical corrections were made and assuming a zero mass quadrupole moment for the Sun) perihelion advance was noted [13]. General Relativity predicts a value of 43.03 ± 0.03 arc seconds per century. This phenomenal agreement was later questioned by proposing that the Sun was oblate and hence had a gravitational quadrupole moment. This quadrupole moment would then contribute to the classical perihelion advance and destory the agreement previously supposed.

There are two approaches to determining the solar quadrupole moment. First, visual oblateness measurements of the Sun can be made and from these determine a quadrupole moment. Second, knowing the perihelion advance of two planets, the different radial dependencies of quadrupole and relativistic effects would allow a separation of these two terms. Visual oblateness measurements have been performed [14] with possibly conflicting results. Establishing a quadrupole moment from a visual oblateness is the weak link in this type of measurement however. The separation of an excess brightness at the pole or equator from a true oblateness complicates the problem. Further, the net quadrupole moment averaged over several years is needed in order to eliminate the

possibility of a periodic fluctuation. Hill and Stebbins [15] cite an oblateness of 18.4 ± 12.5 arc millisec which corresponds to a solar rotation in keeping with the observed equatorial sunspot movement. The relativistic perihelion advance of 43.11 arc seconds/century is calculated including this oblateness of the Sun.

A measurement of the perihelion advance of two or more planets in order to separate the relativistic term from the quadrupole term is a formidable experimental problem. Table 1 gives the relativistic prediction of the perhelion advance of $\delta\tilde{\omega}$ for the four interior planets as well as relative $\delta\tilde{\omega}$ presuming the entire precession of Mercury is due to a quadrupole moment of the Sun. The values of $e\delta\tilde{\omega}$ are also listed where e is the eccentricity of the planet's orbit. The parameter $e\delta\tilde{\omega}$ is the quantity which would be measured if position measurements were made of the planet throughout their orbits.

If observations were made for ten years on Mars, the expected perihelion advance would be 0.013 arc second. A 0.001 arc second accuracy gives only a 8% measurement. This is an unimpressive test compared to other techniques.

Orbiting Gyroscope

An Earth orbiting gyroscope provides an additional test of General Relativity. A precession with respect to an inertial coordinate system of an orbiting gyroscope's axis of rotation is expected. This so called geodetic precession amounts to about 7 arc seconds per year. A special satellite would have to be constructed which would have a sensitive gyro and telescope to establish a coordinate system with respect to

Table 1. Perihelial precession for the minor planets.

Data in seconds of arc per century.

	Relativistic Effect		Quadrupole effect normalized to Mercury = 43.03	
Planet	$\delta\tilde{\omega}$	$e\delta\tilde{\omega}$	$\delta\tilde{\omega}$	$e\delta\tilde{\omega}$
Mercury	43.03	8.847	43.03	8.847
Venus	8.6	0.059	4.81	0.0331
Earth	3.8	0.064	1.55	0.026
Mars	1.35	0.13	0.354	0.033

a set of distant stars. Funding for this program is continuing [16], but, to date, such a satellite has not been launched [17].

Cosmological Theory Verification

There are inconsistencies with observations and some cosmological theories which a time varying gravitational constant, G, would remove. The big bang theory predicts the age of the Universe to be 1.3×10^{10} years [18]. The oldest stars are estimated to be 3×10^{10} years [19]. If the gravitational constant were stronger in the past, stars would have evolved more rapidly than supposed with a constant G and hence this apparent contradiction would be resolved.

Great care must be used in considering a time variation of a fundamental constant. The cosmological problem is perhaps better stated: Was the ratio of the gravitational constant to the electromagnetic constant ε_o or the strong or weak nuclear interaction constant greater in the past than it is now? The cosmological problem supposes a weakening of gravity while the other three constants are fixed. The relative changes are the only measurable quantities as all "clocks" require one of these four interactions for their operation. Throughout the following section time will be understood to mean Cesium clock time.

A change in G would produce a change in the period of the Earth's orbit. This change can be determined to first order by presuming a circular orbit and equating the gravitational attraction of the Earth by the Sun to the centripetal force,

$$m\omega^2 r = \frac{GMm}{r^2} \quad , \tag{2}$$

where M is the mass of the Sun and m, r, and ω are the Earth's mass, orbital radius, and angular momentum, respectively. Then taking a derivative with respect to time, and invoking conservation of momentum, $m\omega r^2$ = constant gives

$$\frac{1}{2} m \omega \dot{\omega} r^3 = \dot{G}Mm \quad . \tag{3}$$

Division by equation 2 reduces this to

$$\frac{\dot{\omega}}{\omega} = -\frac{\dot{p}}{p} = \frac{2\dot{G}}{G} \quad . \tag{4}$$

If $\dot{G}/G$ is -3×10^{-11} per year, the Earth's period P ($P = 1/2\pi\omega$) would change by 6×10^{-11} per year or 1.9×10^{-3} sec/year. The equivalent change in the Earth's position after a nominal year would be 7.8×10^{-5} arc seconds. This effect would be measured in a reasonable observing time by making yearly determinations of the time of solar transit of a group of fixed stars. The first two transits of a star would establish the period P. In subsequent years the time of stellar transit would be changed by

$$\Delta\tau = \int_0^T t\dot{P}\, dt = \frac{T^2}{2} P \quad . \tag{5}$$

Table 2 gives a listing of observing times and expected values of $\Delta\tau$ and Δs assuming $\dot{G}/G = -3 \times 10^{-11}/yr$. There is no experimental reason to expect this value however, and Table 2 also shows the minimum $\dot{G}/G$ detectable with this technique.

The time of solar transit must be known as accurately as the stellar position. Since the star-Sun relative velocity is about 1/24 arc second per second, the time of solar transit need only be known to 0.024 seconds. A measurement of 24 milliseconds represents an accuracy of 7.6 parts in 10^{10}, however. This accuracy is easily within the accuracy limits of a WWVB link to the NBS atomic clock standards. Only this additional information is required. This observational program may be carried on concurrently with other observational programs. Current data on $\dot{G}/G$ data is sketchy. A value of $(-1.5 \pm 2.7) \times 10^{-11}$ yr^{-1} has been reported by Van Flandern [20].

Plane of Ecliptic Tied to Celestial Coordinates

There are two coordinate systems used in astrometry. The first is determined by the plane parallel to the Earth's equator, passing through the Sun's center and its intersection with the plane of the Earth's orbit ecliptic. One point on the line of intersection is the ascending node and from this point right ascension is measured. Declination is measured from the equator to each pole. The other coordinate system uses the plane of the ecliptic and the intersection with a plane parallel to the plane of the equator passing through the Sun. Surprisingly, the relative orientation of these two coordinate systems is much less precisely known than measurements in either coordinate system.

Table 2. $\dot{G}/G$ effects observable versus observing time.

T (yrs)	$\dot{G}/G = -3 \times 10^{-11}/yr$		
	$\Delta\tau$ (sec)	ΔS (arc sec)	min $\dot{G}/G \geq 2\sigma$
5	2.38×10^{-2}	9.8×10^{-4}	6.5×10^{-11}
10	9.5×10^{-2}	3.9×10^{-3}	1.6×10^{-11}
15	0.21	8.8×10^{-3}	7.0×10^{-12}
20	0.38	1.6×10^{-2}	4.0×10^{-12}

Precision solar astrometry could accurately determine their relative orientations. Current uncertainties are about 0.02 arc second [3]; the SCLERA instrument could reduce this to milli arc seconds. This could be done while determining other parameters, e.g., gravitational deflection of starlight, if the proper observing regime were followed.

The application of the SCLERA techniques to nighttime astrometry would have far reaching effects. Improved parallaxes of relatively near stars and parallaxes of additional stars would result. This is important to astrophysical theory. Stars of known trigonometric distance are the only means of calibrating the absolute luminosities and bolometric corrections of the stars. Expanding the sphere of stars of known parallax would expand the number of stars of known parallax. More importantly, different spectral types and luminosities would be included. Increased knowledge of the proper motion of stars would give more knowledge about galactic rotations and velocity dispersions as a function of spectral type. The adaptation of the SCLERA instrument by replacing the Sun detector by another star detector and measuring relative separations of star pairs would result in an order of magnitude improvement in the best known star positions. Optimizing the instrument for the task of detecting low level signals rather than its current optimization for daytime high background noise reduction would allow much fainter objects to be tracked.

CHAPTER 3

EXPERIMENTAL PROBLEM

The experimental problem of measuring a star's position near the Sun presents several technical difficulties. The extent to which these problems can be solved determines how well the experiment can be performed. This chapter will discuss the technique used in determining an object's location and the systematic errors prevalent in such a determination; the difficulties in extracting meaningful astrometric information from object position data; and the availability of celestial objects suitable for daylight astrometry. Each of the above areas are strongly interdependent. For example, the detection technique is dependent on the luminosity of the detected object.

Stellar Tracking

The techniques involved in determining a star's observed position relative to the Sun will now be discussed. The major portion of the astrometric telescope is described in Oleson et al. [4], and this dissertation will not be redundant with that work except as necessary. The problems encountered in determining a stellar position are divided into two categories, those associated with determining the center of the star, and those associated with determining the position of the star's center with respect to other objects. The former problem will be discussed first.

The problems associated with determining the center of a star are removing the lateral chromatic aberration of the atmosphere; being insensitive to the background sky gradient; and most importantly, detecting the star with daytime sky brightness present.

Removal of Lateral Atmospheric Chromatic Aberration

Starlight arriving at the Earth's surface has been deviated from a straight line by the refraction of the Earth's atmosphere. Fluctuations in the index of refraction of the atmosphere cause the direction of the starlight to exhibit a random fluctuation. This random fluctuation is called seeing. For a given wavelength, the position of a star at the focal plane of a telescope is observed to be a two dimensional Gaussian [21]. Thus, for a given wavelength seeing does not affect the center of a stellar image and the accuracy to which a stellar position can be measured depends on the accuracy to which the center of the Gaussian can be found. The profile of a polychromatic star is the superposition of the generalized Gaussians for each wavelength, the centers of which are offset to the extent that the atmospheric refraction varies with wavelength. This effect is the lateral color aberration of the atmosphere. For example, at sea level the positions of a star with a zenith angle of 45° as observed at 7000Å and 4000Å are separated by 1.4 arc seconds. If a polychromatic detector is used to measure a star's position, positional uncertainties result from the lateral color aberration. Ordinarily, this effect is dealt with by limiting the bandwidth of the detector and hence the usable light intensity to the point of making monochromatic measurements.

The obvious advantages of removing the lateral chromatic aberration of the atmosphere is that in so doing, wide bandwidth detectors may be used. Broad bandwidth detectors result in more photoelectrons from both the star and background and hence yield better statistics in equal observing times as compared to narrow bandwidth detectors.

The effect of increased signal on the statistical errors of a star position is given by [22]

$$\frac{\Delta x}{\sigma} = (N_{BG})^{1/2}/N_S \tag{6}$$

where Δx is a positional uncertainty for a unit time of observation. N_{BG} and N_S are the number of background and star photoelectrons generated by the detector per unit time and σ is a scale parameter containing the details of the detection scheme but determined primarily by seeing. For a given signal-to-background ratio

$$\alpha = N_S/N_{BG} \quad , \tag{7}$$

$$\frac{\Delta x}{\sigma} = (N_S/\alpha)^{1/2}/N_S = (\alpha N_S)^{-1/2} \quad . \tag{8}$$

Wider bandwidth furnishes more photoelectrons and hence improves statistical position uncertainties. However, α may vary drastically over the bandwidth in question. α is a function of the star type and detector used. A thorough discussion of bandwidth selection is found in Chapter 4.

To date, instrumental chromatic aberrations are dealt with independently of atmospheric dispersion by the use of reflectors or an achromatic objective in the case of refractors. A Mangin mirror system (see Figure 2) is capable of reducing both of these chromatic problems. In the Mangin mirror system light from the objective comes to a first focus, then passes through a fields lens. The field lens images the objective on the Mangin mirror which is a closely spaced negative lens and concave mirror. The Mangin mirror reflects the light back through the field lens to a final focus. The Mangin mirror system has sufficient degrees of freedom with respect to position and focal lengths of elements to attain a longitudinal chromatic aberration in a 4000-7000Å bandwidth of less than the monochromatic depth of focus of the objective. Further chromatic correction cannot be utilized. A computer-aided parameter fit resulted in the design specified in Chapter 4. For the rest of the chapter the system will be assumed to be achromatic. Atmospheric lateral chromatic aberration can also be reduced by a factor of 10^{-2} by a Mangin system. A general proof of this follows.

Atmospheric Lateral Chromatic Aberration Correction: General Proof. A proof of a Mangin mirror system's ability to correct for the lateral chromatic aberration of the atmosphere was first given by Hill and Zanoni [5]. The following is a derivation which demonstrates the applicability of the geometry used in the SCLERA instrument.

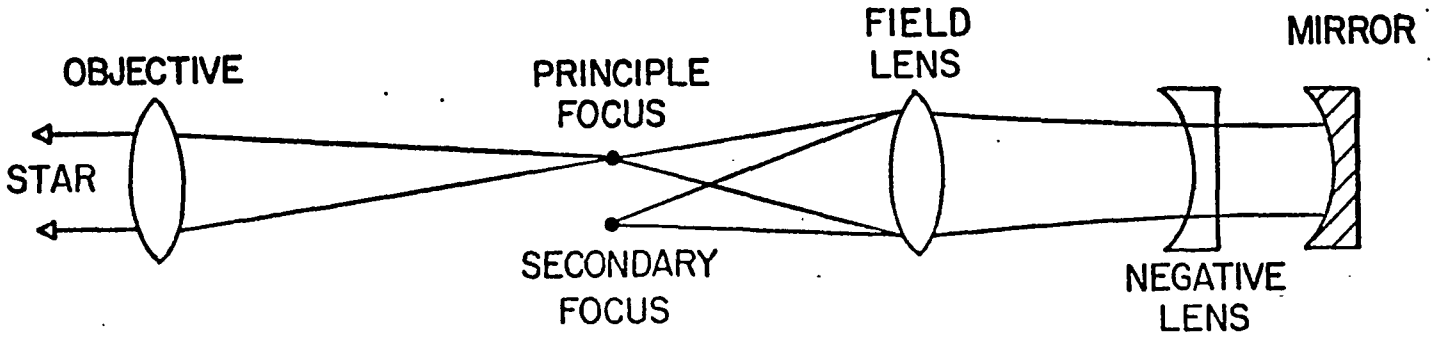

Figure 2. Mangin mirror system.

Different wavelengths of light from a distant point source have slightly different angles of incidence on a telescope objective because of atmospheric refraction. The difference between the vacuum propagation and atmospheric propagation angles of incidence is defined as the atmospheric refraction R. Hill and Zanoni [5] derive this quantity as

$$R = \overline{\delta}_a U_a + \overline{\delta}_w U_w \quad , \tag{9}$$

where $\overline{\delta}_a$ and $\overline{\delta}_w$ are the specific refractivities of air and water vapor, respectively, and U_a and U_w are the path integrals of their respective density gradients. Tacitly, a $\overline{\delta}U$ term could be added for each constituent of the atmosphere.

Starlight of wavelength λ_1 passing through the atmosphere will have a focus S_1 laterally offset from a straight line ℓ_1 passing through the star and the nodal point of the objective (see Figure 3) by

$$h_1 = R(\lambda_1)\ f(\lambda_1) \quad , \tag{10}$$

where h_1 is the lateral offset, λ_1 is the wavelength of the light, and $f(\lambda_1)$ is the focal length of the objective. A Mangin mirror system's optical axis, ℓ_2, is oriented such that it passes through a point Q, the focus of starlight of wavelength λ_o, at an angle θ with respect to ℓ_1. The height of S_1 in object space of the Mangin mirror system is

$$y_1 = R(\lambda_1)\ f(\lambda_1) - \theta\,[a - f(\lambda_1)] - h_o \tag{11}$$

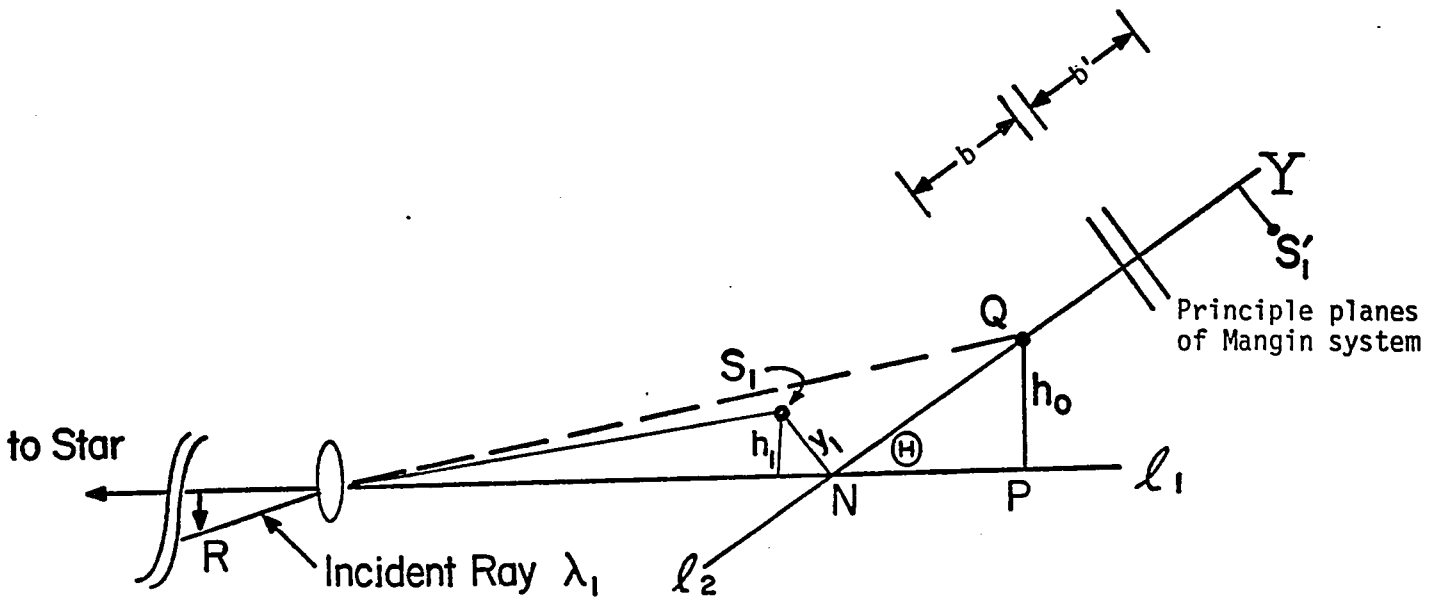

Figure 3. Mangin system geometry.

where h_o is the height at Z and a is the objective-point P separation. The image of y has a height in the image space of the Mangin mirror system of

$$Y = \{R(\lambda_1)f(\lambda_1) - \theta[a - f(\lambda_1)] - h_o\} \cdot \left(\frac{b'}{b+a-f(\lambda_1)}\right) \qquad (12)$$

where b and b' are the distances from the object plane to the primary principle plane and image plane to the secondary principle plane respectively. The Mangin system is designed such that $b' = b$ at $\lambda = \lambda_o$. Sustitutaion of

$$f(\lambda_o) = \frac{1}{\delta_o K} \quad , \qquad (13)$$

where δ_o is the refractivity of the objective and K is the geometrical factor of the objective,

$$Y = \frac{\delta_a U_a + \delta_w U_w}{\delta_o K} - h_o - \theta[a - f(\lambda_1)] \cdot \left(\frac{b}{b+a-f(\lambda_1)}\right) \quad . \qquad (14)$$

By construction $Y(\lambda_o) = 0$, regardless of the value of θ because Q was on the Mangin's optical axis. $Y(\lambda_1)$ can be made to vanish if

$$\theta = \left(\left.\frac{\delta_a U_a + \delta_w U_w}{\delta_o K}\right|_{\lambda=\lambda_1} - h_o\right) \Big/ \{f(\lambda_1) - f(\lambda_o)\} \quad . \qquad (15)$$

In practice, a good fit is assured for all λ in the selected bandwidth if two well-separated wavelengths produce zero final image height. The goodness of fit is a measure of the linearity of δ_a/δ_ℓ versus δ_ℓ. Hill and Zanoni [5] tabulate this for several glasses. Taking an objective of BK-7, focal length 1226.9 cm at 4861Å, and a zenith angle of 45°, a factor of 100 reduction in atmospheric lateral chromatic aberration is achieved. It is to be noted that only two requirements are placed on

the optical specifications of the Mangin mirror. First, the Mangin mirror must bring the final image into a chromatic aberration free focus in the absence of differential atmospheric refraction. Second, the Mangin must have provisions for rotation and lateral displacement with respect to the objective in order to correct for objects of different zenith angles.

Mangin Mirror System Integration into a Telescope. The Mangin mirror system becomes useful to astrometry if a method is devised for selecting α and h_1, and a technique for maintaining them at their appropriate values while a star passes from horizon to horizon. These parameters can be servoed to their proper values if two detectors are used to track a star; one having its spectral response centered at λ_1 and the other at λ_2. Four non-competitive servo systems solve the following equations:

$$P_{\parallel}(\lambda_1) + P_{\parallel}(\lambda_2) = h_{\parallel} \quad , \tag{16}$$

$$P_{\perp}(\lambda_1) + P_{\perp}(\lambda_2) = h_{\perp} \quad , \tag{17}$$

$$P_{\parallel}(\lambda_1) - P_{\parallel}(\lambda_2) = \alpha_{\parallel} \quad , \tag{18}$$

$$P_{\perp}(\lambda_1) - P_{\perp}(\lambda_2) = \alpha_{\perp} \quad , \tag{19}$$

where P denotes the position of the star and the subscripts $\parallel$ and $\perp$ denote two orthogonal directions.

The various $P(\lambda)$'s in the above equations are determined by placing a pinhole at the final focus of the Mangin mirror system. The Mangin mirror system is oriented in coordinates $h_{\parallel}$, $h_{\perp}$, $\alpha_{\parallel}$, $\alpha_{\perp}$ so that starlight in wavelengths λ_1 and λ_2 pass through the pinhole. After passing through the pinhole the light is split into a red component and a blue component corresponding to λ_1 and λ_2, respectively. The stellar image is oscillated in the $\parallel$ and $\perp$ direction and phase sensitive detection is then performed on these two colors in two directions, and this furnishes the signals to servo $h_{\parallel}$, $h_{\perp}$, $\alpha_{\parallel}$, $\alpha_{\perp}$.

Background Shot Noise Limit on Position Accuracy

The accuracy to which the center of a stellar image can be determined is limited by, among other things, background shot noise. In his dissertation, Zanoni [22] calculated this limit; the following is a synopsis of that calculation. The background entering a telescope of aperture D is given by

$$N_B = 2.3 \times 10^{10} AD^2 \qquad (20)$$

where N_B is the number of photons per second of time per square arc second in a 3000-6000Å bandwidth and A is the relative sky to Sun brightness. At SCLERA, $A \approx 10^{-5}$. For a 10 cm aperture,

$$N_B = 2.3 \times 10^{7} \text{ photons sec}^{-1} \text{ (arc sec)}^{-2} . \qquad (21)$$

The number of photons per second for a star of visual magnitude m, for a telescope of aperture D, is

$$N_S \approx \frac{8 \times 10^5 \, D^2}{(2.5)^m} \quad . \tag{22}$$

For a 10 cm aperture

$$N_S \approx \frac{8 \times 10^7}{(2.5)^m} \quad . \tag{23}$$

Assuming a 0.5 transmission factor and a quantum efficiency of ε for the photodetector, the number of photoelectrons per second from the star (SPE) and the background (BPE) are, respectively,

$$N_{SPE} = \frac{4 \times 10^7 \, \varepsilon}{(2.5)^m} \tag{24}$$

and

$$N_{BPE} = 8.6 \times 10^6 \, \varepsilon \, 4R^2 \quad , \tag{25}$$

where R^2 is the radius in arc seconds of the detector pinhole.

Assuming a one arc second pinhole radius and a quantum efficiency of 0.2 for the given bandwidth, the value for N_{SPE} and N_{BPE} are

$$N_{SPE} = \frac{8 \times 10^6}{(2.5)^m} \tag{26}$$

and

$$N_{BPE} = 1.7 \times 10^6 \quad . \tag{27}$$

The spatial light distribution in the stellar image is assumed to be of the form

$$N_S(x,y) = N_{SPE} \frac{\exp[-(x^2+y^2)/2\sigma^2]}{2\pi\sigma^2} \quad , \tag{28}$$

where σ^2 is the variance of stellar-photon distribution; for daytime conditions $\sigma \approx 2$ arc seconds typically. Using the first derivative of the light distribution to lock onto the star, the sensitivity of the detector is

$$\Delta N_{SPE} = \frac{N_{SPE}}{2\pi\sigma^2} \left(\frac{\Delta X}{\sigma}\right) \frac{\partial}{\partial X} \int_{-\infty}^{\infty} dy \int_{\sigma/2 - X/\sigma}^{\sigma/2 + X/\sigma} e^{-(x^2+y^2)/\sigma} \, dx \quad , \tag{29}$$

$$\Delta N_{SPE} = \frac{\sqrt{2/\pi e}\, N_{SPE}}{\sigma} \left(\frac{\Delta X}{\sigma}\right) \quad , \tag{30}$$

where X is the displacement of the detector with respect to the stellar image. If T is the integrating time of the detector,

$$\Delta N_{BPE} = (N_{BPE}/2T)^{1/2} \quad . \tag{31}$$

Equating N_{BPE} and N_{SPE} gives a rms value of $\Delta X/\sigma$,

$$\frac{\Delta X}{\sigma} = \frac{\sigma^2 \sqrt{Xe}}{2} (N_{BPE}/T)^{1/2} / (N_{SPE}) \quad . \tag{32}$$

Combining Equations 26, 27, and 32 results in

$$\frac{\Delta X}{\sigma} = 7.4 \times 10^{-4} (2.5)^m T^{-1/2} \quad . \tag{33}$$

Table 3 gives ΔX for stars of first to sixth magnitude and integrating times of 1 to 1000 seconds.

Background Sky Brightness Gradient Effect

The background sky brightness near the Sun exhibits a gradient, becoming brighter near the Sun. The scattered light from the instrumental sources have a similar gradient. A first harmonic method of star detection is offset from the true star position by this gradient. The position offset of the detector is given by

$$\Delta X = \frac{\nabla N_{BPE} \cdot S\sigma}{N_{SPE}} \quad , \tag{34}$$

where ∇N_{BPE} is the spatial gradient in the number of background photoelectrons and S is the detector scan amplitude. The sky brightness and instrumental gradient has been measured to be

$$\frac{\nabla N_{BPE}}{N_{BPE}} = 3 \times 10^{-3} \text{ per arc second} . \tag{35}$$

Combining this with Equations 27, 28, and 35 gives

$$\Delta X = 1.6 \times 10^{-2} \, (2.5)^{m} \text{ arc seconds} . \tag{36}$$

For a sixth magnitude star this is 3.9 arc seconds. Two pinholes situated beside the star detector pinhole are used to generate a signal proportional to the gradient. The two pinholes are equidistant from the star pinhole and determine a line nearly perpendicular to the gradient. This arrangement furnishes a background gradient signal which

Table 3. Tracking accuracy in $\Delta x/\sigma$ for various stellar magnitudes and integrating times.

Taken from Zanoni [22].

Visual Magnitude m	Integrating Time T in Seconds			
	1	10	10^2	10^3
1	7.1×10^{-3}	2.3×10^{-3}	7.1×10^{-4}	2.3×10^{-4}
2	1.8×10^{-2}	5.7×10^{-3}	1.8×10^{-3}	5.7×10^{-4}
3	4.5×10^{-2}	1.4×10^{-2}	4.5×10^{-3}	1.4×10^{-3}
4	0.11	3.3×10^{-2}	1.1×10^{-2}	3.3×10^{-3}
5	0.38	8.5×10^{-2}	3.8×10^{-2}	8.5×10^{-3}
6	0.70	0.22	7×10^{-2}	2.2×10^{-2}

is invariant to rotations to second order in the gradient. This signal is subtracted from the signal produced by the star detector pinhole. Since the background gradient detectors are not restricted in aperture by optimization of the star detector sensitivity, larger pinholes are used here in order to reduce background shot noise. The combined background aperture is 20 times larger in area than the star detector aperture. This reduces the shot noise of the difference to only 2.5% more than the star pinhole alone.

The background light (both sky and instrumental) can be represented over a small segment of the field by $I = A + Bx$. The signal produced by the star detector is then

$$V_s = g_s[(A+Bx) + f_s(x,\text{scan})] + O_s \tag{37}$$

and by the background detector is

$$V_b = g_b(A+Bx) + O_b \tag{38}$$

where v_s and v_b are output signals from the star and background detectors, g_s and g_b are the gains, O_s and O_b are the instrumental offset of each detector, and $f_s(x)$ is the starlight distribution. Removal of the background gradient requires scanning the star and background at two amplitudes; a low amplitude scan in which the star signal is present and a large amplitude scan which removes most of the star signal and increases background gradient signal. σ and 3σ are chosen. At 3σ

the star signal is down by a factor of about 2×10^{-2}. Combining Equations 37 and 38 results in

$$V_s = \frac{g_s}{g_b} V_b + O_s - \frac{g_s}{g_b} O_b + g_s f_s(x,\text{scan}) \quad . \tag{39}$$

At scan = 3σ, $f_s \approx 0$ and g_b is servoed until first harmonic in $V_s - \frac{g_s}{g_b} V_b$ is zero. At scan = σ, X is servoed again using $V_s - \frac{g_s}{g_b} V_b$ as the error signal. The fact that there is a residual f_s term in the 3σ scan servo error signal is of no consequence if both servos are operated iteratively in time.

This background gradient removal technique does not require identical spectral responses of the two detectors. This is a necessary condition because it is unlikely that a matched pair of detectors could be obtained with the necessary high gain at the red end of the spectrum. It is sufficient to note

$$g_s = \int_{\lambda_1}^{\lambda_2} g(\lambda)\ N(\lambda)\ d\lambda/N \tag{40}$$

where λ_1 and λ_2 are the detector cutoff wavlengths , $N(\lambda)$ is the wavelength distribution of photons, N is the total number of photons of the certain portion of the sky being scanned and $g(\lambda)$ is the photomultiplier spectral response. A variation in the background gradient as a function of wavelength results in a change in g and a different A/B ratio for the two detectors. The difficulty associated with different A/B ratio is that an incomplete subtraction of the D.C. component of

the signal's results. A correction for this is made by introducing an instrumental offset. The time spent in large scan versus small scan is determined by minimizing the sum of the statistical errors in a measurement of the star position and in a measurement of the background sky gradient. About 90% of the time is spent in the small scan mode and 10% in the large scan mode. This ratio is relatively unaffected by the magnitude of the star being tracked.

This method of removing the background gradient is subject to errors due to higher order terms in the gradient approximation used in the previous calculation. If a $1/R^2$ model of the background intensity is assumed, where R is the distance from the limb of the Sun, higher order terms result in an error of 1 part in 10^4 or 0.38 milli arc seconds in the position of a sixth magnitude star.

Determination of Star-Sun Separation

The position of a star's image with respect to that of the Sun is measured interferometrically. At the principle focus of the SCLERA instrument one second of arc = 56 μm. A 0.001 arc second measurement requires a measurement to 56 nm. An interferometer which is capable of determining the direction of motion in order to track the statistical motions of a star is needed.

Alignment of the star detector pinhole and the measuring interferometer is critical. The longitudinal position of the pinhole along the interferometer line only adds a constant to the measured distance. This can be removed at the time of data reduction. Another term arising from a lateral offset has the same radial dependence as a gravitational

deflection. If the pinhole is located at a point p (see Figure 4), a distance δ from the star-Sun interferometer line S-S' the Pythagorean relation

$$(R + \varepsilon)^2 = R^2 + \delta^2 \tag{41}$$

holds where ε is the error introduced into the measurement at a measured distance R. To second order in δ^2,

$$\varepsilon = -\frac{\delta^2}{2R} \quad . \tag{42}$$

For an error of 10^{-3} arc seconds at one solar radius $\approx$ 1000 arc seconds, δ is 1.4 arc seconds or 75 μm (0.003 in). This accuracy is well within machining tolerances. This misalignment could be corrected in the initial data taking phase of telescope use. If the position of the pinhole were varied as a star was tracked near the Sun, the position which gave the minimum star-Sun distance after data reduction would be the correct position.

A stabilized He-Ne laser is used as a light source and the interferometer uses a quadruture detector which is capable of determining the direction of motion and has a resolution of $\lambda/8$, 79.1 nm. See Chapter 4 for a description. Statistical methods are used to gain accuracies better than the 56 nm requirement.

Determination of Stellar Position

This section discusses the accuracy to which stellar or planetary positions can be determined from data obtained by tracking them

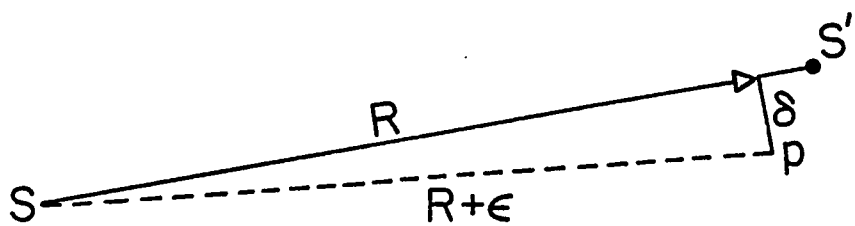

Figure 4. Star pinhole offset.

as they pass the Sun. Experimentally the position of the stellar image R_S and the near and far edges of the Sun R_s^+ and R_s^-, respectively, which lie along the star-Sun line are measured. The distance R between the stellar and solar image s is given by

$$R = [R_S - (R_s^+ - R_s^-)/2]\ [R_s^+ + R_s^-)/(\overline{R}_s^+ + \overline{R}_s^-)]^{-1} \qquad (43)$$

where the sign convention is determined by measuring distances from the center of the Sun. The factor $(R_s^+ + R_s^-)/(\overline{R}_s^+ + \overline{R}_s^-)$ is present because the solar diameter is used to correct for scale changes where $\overline{R}_s^+$ and $\overline{R}_s^-$ are mean values of R_s^+ and R_s^-, respectively.

It would appear that in order to measure the gravitational deflection of starlight or establish the plane of the earth's orbit it would be sufficient to measure R as a function of time. This is not true however because any uncertainty in stellar latitude appears in a form identical to that of gravitational light deflection. Let G be the gravitational light deflection coefficient, b_o the stellar latitude distance for large star-Sun distances (impact parameter), $\omega(t)$ the instantaneous angular orbital velocity of the earth calculated from orbital parameters, and t_o the time the star and Sun have the same celestial longitude, i.e., conjunction. The equation

$$R\text{-}G/R = \{b_o^2 + [\int_{t_o}^{t} \omega_t(t)\ dt]^2\}^{1/2} \qquad (44)$$

relates these quantities. If a value $b = b_o + \varepsilon$ is substituted into the above equation and ω assumed to be a constant, then to first order in ε,

$$R - G/R = [b_o^2 + \omega^2(t-t_o)^2]^{1/2} + b_o \varepsilon/R \quad . \qquad (45)$$

Therefore, a measurement of R alone does not determine either G or b_o.

There are several possible ways to make meaningful determinations of G or b_o by knowing $R(G,b_o,t)$ and additional information. If G were known to 1% as is currently claimed [2], there would be little trouble in determining b to 0.001 arc second for objects having a minimum b of about 20 seconds. Determination of G is the more urgent problem which dictates reducing errors due to uncertainties in b_o.

If b_o were small with respect to $R_\odot$ the 0.05 arc second uncertainty in star-ecliptic measurements [23] would have vanishingly small effect on a determination of G. Inspection of Table 4 shows the smallest b_o for 6 mag or brighter stars is 0.725 minutes of arc. This results in 0.022 arc second uncertainty in $G/R_\odot$,

$$\begin{aligned} b_o\varepsilon/R_\odot &= (22 \text{ arc sec} + 0.05 \text{ arc sec})/1000 \text{ arc sec} \\ &= 0.022 \text{ arc sec} \quad . \end{aligned} \qquad (46)$$

The gravitational deflection at the limb $G/R_\odot$ is 1.75 arc seconds. Using this results in a 1.3% error. The next smallest usable b_o results in a 1.8% error and the rest are over 2%.

If a pair of stars of known separation, $d\pm\xi$, where d is their separation and ξ is the uncertainty in that separation, were tracked

Table 4. Stars near the plane of the ecliptic.

RA(1975)	PMRA	DEC(1975)	PMDEC	MIN FROM ECL.	VMAG	SPT	GCNO	DM NO
0 24.13	-0.0010	1 48.09	-0.012	-40.831	6.0	G5	1010	1 57
0 47.05	0.0506	5 9.62	-1.142	20.671	5.8	G5	1019	4 123
1 12.42	0.0095	7 26.64	-0.050	6.178	5.6	A5	1033	6 174
1 49.54	-0.0049	10 55.23	-0.022	3.297	5.9	F0	2229	10 252
2 43.17	-0.0002	15 12.43	-0.016	-13.547	5.8	B8	3303	14 457
2 50.11	0.0022	14 58.82	-0.024	-59.220	5.5	B5	1079	14 480
3 40.87	0.0001	19 37.31	-0.010	13.211	5.5	B6	4430	19 578
4 15.80	-0.0031	20 31.14	-0.057	-42.191	4.8	A3	5172	20 724
4 17.96	0.0022	21 5.03	-0.040	-14.127	5.4	B5	5210	20 733
4 16.91	0.0068	21 31.21	-0.034	14.879	5.6	A5	5189	21 618
4 18.13	0.0022	21 42.91	-0.038	23.298	5.3	A0F	5216	21 623
4 22.07	0.0012	20 55.54	-0.027	-34.339	5.9	B8	5317	20 751
4 23.88	0.0070	22 14.32	-0.046	39.836	4.4	A3	5350	21 642
4 23.93	0.0079	22 8.68	-0.052	34.080	5.4	F0	5351	21 643
4 26.53	0.0069	21 33.97	-0.036	-7.098	5.7	A5	5412	21 647
4 40.75	-0.0001	22 54.65	-0.016	41.229	4.3	B5	174	22 739
5 33.93	0.0005	24 1.50	-0.014	33.338	5.3	B3	6916	23 954
5 47.49	0.0000	24 33.67	-0.027	58.454	5.0	K0	7283	24 970
5 55.41	0.0002	24 14.87	0.000	37.834	6.0	B3	7483	24 1033
6 2.60	-0.0004	23 16.04	-0.102	-21.197	4.3	G5	1163	23 1170
6 8.22	0.0006	23 7.16	-0.002	-29.250	5.8	B1	7827	23 1226
6 10.01	-0.0002	24 25.68	-0.055	49.703	5.9	K0	7672	24 1151
6 21.45	0.0040	22 31.74	-0.112	-59.380	3.2	M0	241	22 1304
6 24.03	-0.0006	23 20.57	-0.024	-8.972	6.0	A0	8290	23 1347
6 50.49	-0.0028	23 37.99	-0.011	34.916	5.8	K5	8976	23 1518
7 3.81	-0.0003	22 40.60	-0.015	-2.149	5.9	A0	9337	22 1566
7 18.64	-0.0018	22 1.81	-0.014	-12.900	3.5	F0	279	22 1645
7 21.97	-0.0015	22 59.73	-0.038	52.191	6.0	A0	9844	23 1698
7 26.26	-0.0040	21 29.93	-0.124	-28.178	5.3	F5	9957	21 1602
7 54.21	-0.0013	19 57.11	-0.043	-47.832	5.4	A0	10707	20 1946
8 21.94	-0.0037	18 24.85	-0.031	-49.233	5.9	F0	1220	18 1930
8 30.18	-0.0040	18 10.84	-0.060	-32.926	5.6	M0	11659	18 1963

Table 4, continued.

RA(1975)	PMRA	DEC(1975)	PMDEC	MIN FROM ECL	VMAG	SPT	GCNO	DM NO
8 43.27	-0.0012	18 14.95	-0.233	22.327	4.2	K0	326	18 2027
8 53.98	0.0001	17 19.66	0.005	11.483	5.9	N8	12322	17 1973
9 13.86	-0.0028	15 2.79	-0.013	-37.018	5.6	K0	12758	15 2009
9 42.38	0.0002	14 8.22	-0.007	47.362	5.6	M0	1252	14 2136
9 56.89	-0.0017	12 33.90	-0.020	28.620	5.2	A0	13724	13 2183
10 7.05	-0.0170	12 5.41	0.003	54.854	1.3	B8	380	12 2149
10 23.94	0.0007	8 54.77	-0.041	-42.039	5.9	M0	14301	9 2351
10 26.33	0.0004	9 53.44	-0.002	30.179	5.9	A0	14361	10 2152
10 31.50	-0.0006	9 26.15	-0.006	32.352	3.9	B0P	396	10 2166
10 33.73	-0.0038	8 46.81	-0.010	5.812	5.7	A0	14541	9 2374
10 54.73	-0.0016	6 19.15	-0.012	-19.044	6.0	M8	15032	6 2369
10 59.46	-0.0034	6 14.18	-0.029	4.106	5.1	A5	15130	6 2384
11 26.66	0.0011	2 59.65	-0.017	-25.831	5.2	K0	1297	3 2504
11 33.10	-0.0123	3 12.00	-0.107	25.994	5.8	F5	15867	3 2521
11 49.38	0.0494	1 54.45	-0.275	48.778	3.8	F8	445	2 2489
13 31.65	-0.0023	-10 2.19	-0.041	-50.376	5.4	G5	18309	-9 3711
14 17.76	-0.0013	-13 15.43	0.024	6.116	4.6	A2	1371	-12 4018
14 49.31	-0.0070	-15 53.64	-0.072	0.725	5.3	E5	1387	-15 3965
14 49.50	-0.0075	-15 56.31	-0.071	-1.071	2.9	A3	548	-15 3966
15 5.23	-0.0031	-16 9.66	-0.025	55.162	5.3	K0	20311	-15 4026
15 31.18	-0.0017	-19 35.19	-0.042	-46.337	5.5	A2	20878	-19 4135
15 37.47	0.0059	-19 13.23	-0.080	-1.278	5.5	G5	21031	-18 4118
15 40.51	-0.0027	-19 35.91	-0.107	-13.111	5.0	K5	1413	-19 4188
15 51.88	-0.0008	-20 5.62	-0.027	-4.042	5.1	B3	1415	-19 4249
15 53.56	-0.0012	-19 18.63	-0.024	48.415	5.9	B5	21364	-18 4195
15 56.21	-0.0012	-20 54.71	-0.021	-39.149	5.9	B5	21420	-20 4364
16 3.98	-0.0004	-19 44.30	-0.021	55.269	2.9	B1	597	-19 4307
16 3.99	-0.0014	-19 44.10	-0.023	55.493	5.1	B1	21610	-19 4308
16 5.35	-0.0007	-20 36.17	-0.024	7.461	4.1	B2	21639	-20 4405
16 5.94	0.0029	-20 48.14	-0.041	-2.756	4.6	G0	21659	-20 4408
16 30.65	0.0009	-21 24.89	0.034	26.090	4.6	F0	22221	-21 4381

Table 4, continued.

RA(1975)	PMRA	DEC(1975)	PMDEC	MIN FROM ECL	VMAG	SPT	GCNO	DM NO
16 55.29	-0.0003	-23 6.73	-0.001	-25.524	5.6	A0	22824	-22 4249
17 24.85	0.0000	-24 9.20	-0.116	-48.515	4.3	F0	1457	-24 13337
17 29.89	0.0003	-23 56.70	-0.028	-31.588	4.9	A0	23717	-23 13412
17 58.27	0.0002	-23 48.92	-0.043	-11.635	4.8	A0	24483	-23 13731
18 0.39	-0.0002	-22 46.89	-0.009	50.430	5.7	B0	24526	-22 4503
18 1.32	0.0004	-24 17.03	-0.009	-39.732	5.5	A5	24555	-24 13793
18 2.34	0.0002	-24 21.78	0.002	-44.531	5.9	DE5	24574	-24 13814
18 10.20	0.0013	-23 42.47	-0.020	-6.549	5.1	K0	24799	-23 14047
18 32.37	0.0002	-24 3.17	-0.010	-39.955	5.7	K2	25336	-24 14472
18 37.00	-0.0002	-23 31.67	-0.020	-12.776	5.8	B9	25475	-23 14572
18 44.84	0.0022	-22 25.21	0.000	45.073	5.8	K2	25687	-22 4854
18 52.66	0.0007	-22 46.64	-0.010	13.424	5.0	G5	25918	-22 4907
18 53.61	0.0074	-22 42.26	-0.026	16.472	5.0	K0	25939	-22 4915
18 54.50	-0.0001	-23 12.43	-0.009	-14.998	5.9	B8	25963	-23 14844
18 56.91	-0.0016	-22 33.88	0.017	19.966	6.0	A2	26039	-22 4928
19 3.19	0.0057	-21 46.77	-0.060	57.025	3.9	K0	26224	-21 5237
19 19.14	-0.0011	-22 27.06	0.035	-13.402	5.5	A5	26664	-22 5063
19 24.83	0.0024	-21 49.67	0.000	11.663	5.6	K0	26623	-22 5105
19 29.42	0.0008	-21 21.94	-0.017	28.860	6.0	A2	26933	-21 5410
20 17.96	0.0004	-19 11.88	-0.006	16.329	5.5	K0	28233	-19 5776
20 25.90	0.0009	-18 17.70	-0.010	42.009	5.2	B6	28442	-18 5685
20 38.63	-0.0015	-18 13.67	-0.018	-2.526	5.3	M0	773	-18 5738
20 53.39	-0.0037	-18 1.14	-0.018	-50.462	5.9	K0	29164	-18 5805
20 56.28	0.0035	-16 7.74	0.002	50.581	6.0	A3	1548	-16 5741
21 4.55	0.0058	-17 19.98	-0.056	-57.853	4.2	A0	1552	-17 6174
21 14.37	0.0017	-15 16.60	0.007	20.841	5.5	M0	29727	-15 5935
21 40.20	-0.0084	-14 9.47	-0.304	-37.534	5.3	G5	30354	-14 6102
22 9.29	0.0020	-11 41.33	0.012	-43.004	5.4	B5	31021	-12 6196
22 51.31	0.0005	-7 42.81	0.039	-44.368	3.8	M0	864	-8 5968
23 18.10	0.0133	-5 15.67	-0.016	-58.003	5.7	F2	32468	-5 5966
23 53.50	-0.0031	-0 1.78	-0.007	41.960	6.0	M8	33165	-0 4585

Table 4, continued.

Taken from General Catalogue of 33342 Stars for the Epoch 1950, Ref. [24]. Precessed to 1975 and prepared by Roger Tibbits of Teledyne Brown Engineering, Huntsville, Alabama.

Explanation of abbreviations:

RA(1975)	Right Ascension in hours and minutes precessed to 1975
PMRA	Proper Motion Right Ascension in minutes per year
DEC(1975)	Declination in degrees and minutes for 1975
PM DEC	Proper Motion Declination in minutes of arc per year
MIN FROM ECL	Minimum distance between star and ecliptic in minutes of arc
VMAG	Visual Magnitude
SPT	Spectral Type
GCNO	General Catalogue Number
DMNO	Durchmusterung Number

separately or simultaneously, use could be made of the increased accuracy of known star separations.

A pair of stars lying on opposite sides of the ecliptic provide the best case in terms of accuracy obtainable. Measuring their relative celestial longitude by noting their times of solar transit (t_i, t_j) results in a determination of the stars relative celestial latitude, α. Let $\sin \alpha = \int_{t_i}^{t_j} \omega_e(t)dt/d$ and $\cos \alpha = (b^i - b^j)/d$ where $\omega_e(t)$ is the Sun's apparent velocity with respect to the stars. If b_o^i and b_o^j are the actual positions of a pair of stars,

$$b_o^i - b_o^j = b^i - b^j + \xi \quad . \tag{47}$$

Introducing this information into Equation 45, two equations are obtained:

$$G/R_i = R_i - \{(b_o^i)^2 + [\int_{t_{i,0}}^{t} \omega_e(t)\, dt]^2\}^{1/2} - b_{i,0}\, \varepsilon/R_i \, , \tag{48}$$

$$G/R_j = R_j - \{(b_o^j)^2 + [\int_{t_{j,0}}^{t} \omega_e(t)\, dt]^2\}^{1/2} - b_{j,0}(\varepsilon+\xi)/R_j . \tag{49}$$

Removing ξ from the equation yields:

$$\begin{aligned} \frac{G(b_{i,0}-b_{j,0}) + \xi b_i b_j}{R_i R_j} &= \frac{R_j}{R_i} b_{i,0} - \frac{R_i}{R_j} b_{j,0} \\ &+ \{(b_o^j)^2 + [\int_{t_{j,0}}^{t} \omega_e(t)\, dt]^2\}^{1/2} b_{i,0}/R_i \\ &+ \{(b_o^i)^2 + [\int_{t_{i,0}}^{t} \omega_e(t)\, dt]^2\}^{1/2} b_{j,0}/R_j \quad . \end{aligned} \tag{50}$$

The extracted terms $(Gb_{j,0})/(R_iR_j)$, $(Gb_{i,0})/(R_iR_j)$, and $(b_{i,0}b_{j,0}\xi)/(R_iR_j)$ have the same $1/R_iR_j$ dependence and have an indistinguishable effect on the measurement of R. However, for selected star pairs $\xi \sim 0.010$ arc second, and the resultant uncertainty of G using this method is about 0.5%, for a pair of stars separated by 3/4° equidistant from the plane of the ecliptic. Better results can be gotten by measuring star pairs lying closer to the ecliptic, but these are few in number.

The SCLERA instrument could be outfitted with two star detectors and perform a nighttime measure of stellar separations to at least its daytime limit of 0.001 arc second. Using this value of ξ, G could be measured to 0.05%. Additionally, other nighttime astrometry programs could be coordinated to furnish the required relative declinations.

Tracking planets could also be used to remove uncertainties in determinations of G/R. Here an analytic expression selecting the impact parameter for each of several transits could be used rather than measuring several independent objects. Tracking planets is useful for a more accurate determination of their orbital parameters. An observational program could be established which acquired sufficient data for both determinations simultaneously. The detection scheme used for planets would differ substantially from that of detecting stars. The difference stems from the fact that a planet is an extended source with time varying structure as opposed to the point source of a star.

Availability of Trackable Stars

The availability of sufficient bright stars to perform the required observations has been tacitly assumed throughout the preceding portion of this chapter. A cataloging of the stars in Table 4 shows that there are about 100 stars sixth magnitude or brighter within 1° of the ecliptic. As might be expected, the distribution is heavily weighted towards the larger magnitudes. There are, however, about 25 fifth order or brighter stars within 1° of the ecliptic. These stars would of course be tracked in preference to other stars.

The star acquisition process requires an accurate predetermination of its position. The star detector scans 5 x 5 arc second sections of the sky. There is no information to determine where the star tracker should be repositioned to acquire a star which is not in the scanned area.

CHAPTER 4

TELESCOPE CONSTRUCTION

This chapter discusses the construction of the telescope. The design is extensively described by Oleson et al. [4], but a brief overview will be provided to give a context for the specific details of the star tracking apparatus.

The telescope is a 12 cm, f/100 refractor, maintained in a vertical position; pointing is accomplished by two mirrors in an elevation-azimuth (el-az) coordinate system. The entire telescope can be evacuated to eliminate instrumental seeing, but to date it has not been used that way. The principal focus is about 12.2 meters below the objective. In this surface are situated the solar primary tracker and solar edge detector package and the star detector. The primary tracker is servoed to track the Sun by furnishing positional error signals to the el-az mirrors. The actual position of the Sun is determined by another detector which scans its edges on the diameter determined by the star-Sun center line. An independent star detector is servoed to track a star as it passes near the Sun. The star detector is also servoed to remove atmospheric lateral chromatic aberration. The star detector is coarsely positioned by a precomputed star position. The star-Sun distance is interferometrically measured and the interferometer alignment is also servoed.

The apparatus description lends itself to division into five parts, each being covered by a section of this chapter. They are: (1) the mechanical considerations of the system, (2) the optical elements, (3) the electronics, (4) the computer and software, and (5) the laser interferometer.

Mechanical Construction

The function of the mechanical assembly is to support and position the star detector apparatus. Of critical importance is the positioning of the star detector in the field of the telescope objective and smoothly moving it to track a star. The rotations of the Mangin system necessary for the removal of atmospheric lateral chromatic aberration must be accommodated. Also, the star-Sun interferometer must be rotated to maintain proper alignment. To fulfill these requirements, the apparatus shown in Figure 5 was used. The star detector apparatus is vertically positioned in the plane of the principal focus of the objective at λ_o by temperature-controlled Invar rods suspended from the plane of the nodal point of the objective. These Invar rods attach to the star detector in the plane of the principal focus. A pair of leaf springs connect the Invar rods to the support for the pinhole which determines the vertical position of the star detector. The leaf springs are attached in a self-compensating arrangement such that the thermal expansion of the springs does not change the height of the pinhole. The springs are required to be at the same temperature, however, and this is assured by being in thermal contact with the temperature controlled Invar parts. The support mechanism maintains a constant field

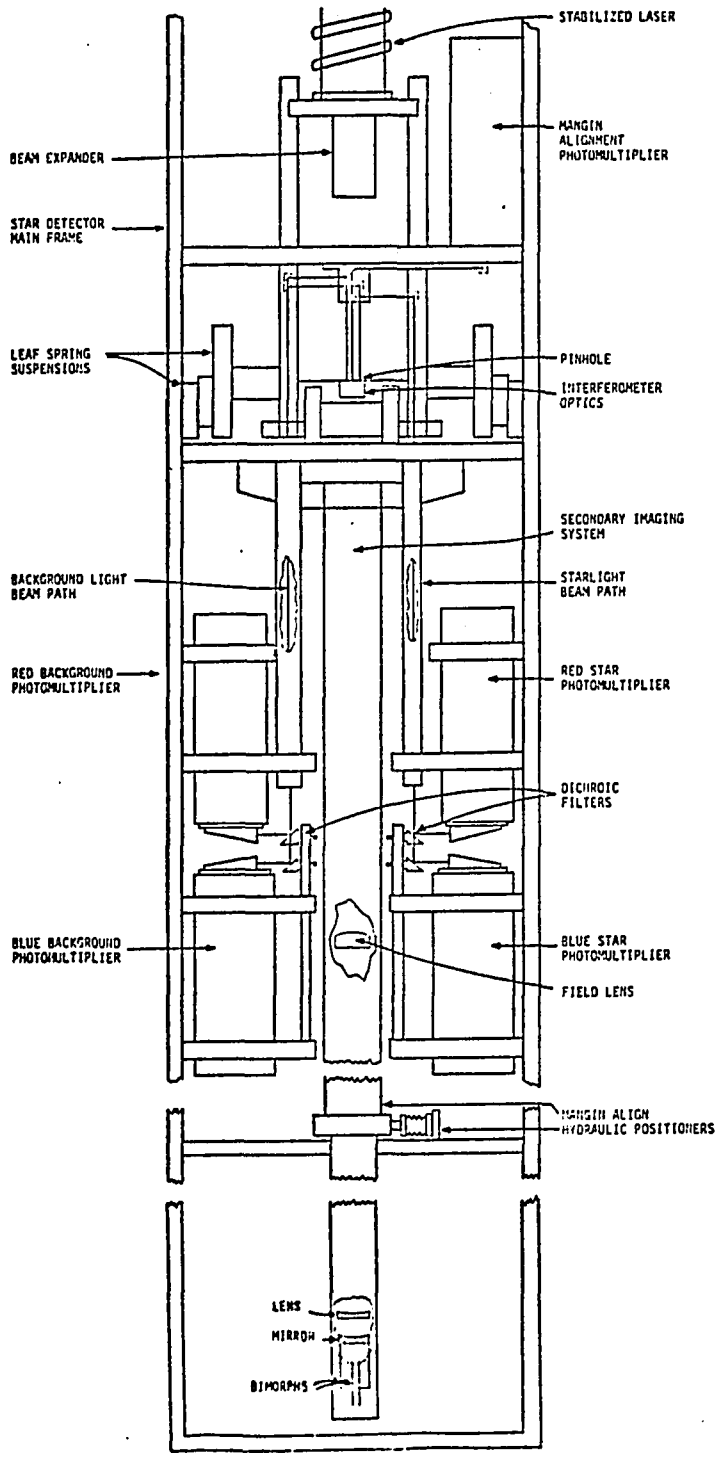

Figure 5. Star detector mechanical assembly.

scale to one part in 10^7. Positioning in the horizontal plane is achieved by attaching the star detector to three lead screws which are in turn attached to the telescope frame. A polar coordinate system is used. Movement in ρ (local star detector-Sun detector axis) is accomplished by movement of the lead screws. Motions in θ (local normal to star detector-Sun detector axis) are accomplished by rotating the entire telescope except the el-az mirrors and the windows.

The pinhole system established the point to which the star image is servoed. Five pinholes and a slot are machined into an Invar plate. The plate is thick enough to provide sufficient thermal conductivity for the temperature-stabilized carrier to maintain dimensional stability. The areas around the pinholes are relieved to 0.025 cm (0.010 in) thick to prevent loss of hole definition upon rotation of the pinhole assembly. This rotation is required for interferometer alignment as discussed in the next paragraph. Hole sizes for background light, Mangin alignment, and star image pinholes are determined in Chapters 3 and 4. The slot allows the unfocused primary field into the Mangin System.

Attached to the pinhole system is the beam splitter and reference corner cube of the Sun detector-star detector distance measuring interferometer. The pinhole, beam splitter, and reference corner cube are precisely maintained in relative position by attaching each to a temperature controlled Invar framework. The reference corner cube is positioned far enough below the beam splitter so that its conjugate point can be superimposed upon the corner cube in the Sun detector apparatus. This condition is necessary for obtaining a white light interferometer

fiducial which is used as the zero point of the star-Sun distance measuring interferometer.

The outgoing beam from the star-Sun interferometer passes below the pinhole platform and the returning beam passes above it allowing the distance determination to be in the plane of the pinhole platform.

The Mangin system, discussed later in this chapter (see Figure 14), is supported by a spring pivot which allows it to rotate with respect to the star detector and is pointed at the nodal point of the objective. Positioning of the Mangin tube is under servo control through hydraulic positioning transducers.

Attached to the star detector frame are five photomultipliers which receive the red star signal, red background signal, blue star signal, blue background signal, and the Mangin align signal. For accessibility, these are positioned along the sides of the detector and the light from the respective pinholes is directed to the photomultiplier using prisms. The prisms are AR coated on the entrance and exit faces and total internal reflection is used on the back surfaces.

Light from the star pinhole passes through two prisms and then through a lens which reconverges the beam. A dichroic beam splitter diverts the red portion of the spectrum to a beam insertion prism optically bonded to the red sensitive PMT (see Figure 5). The beam insertion prism introduces the light at an angle larger than that required for total internal reflection. The photocathode bonded to the inside of the envelope causes total internal reflection. Those photons passing into the photocathode have an increased path length and hence increase

the probability of producing a photoelectron by nearly the same amount. The thickness of the photocathode is not increased; hence the photoelectrons are no more susceptible to recapture than at normal incidence. Those photons not passing into the photocathode on their first reflection are reflected by the outside of the envelope and strike another portion of the photocathode. The effect of this procedure is to increase the overall quantum efficiency of the system. The blue portion of the starlight passes through the beam splitter and is directed into the blue sensitive PMT using another beam insertion prism.

The background light signals pass through a similar set of optics with the exception that there are two beams. These two beams are merged at the PMT surface.

The light from the Mangin align pinhole is diverted to the Mangin align PMT by two prisms. The light level is sufficient not to require a beam insertion prism.

At the bottom of the star detector is a servo motor capable of rotating the star detector slightly about its vertical axis so that the interferometer can be aligned to point at the apex of the Sun corner cube in the horizontal plane. The pinhole system and the attached portion of the interferometer rotate about a horizontal axis perpendicular to the Sun detector-star detector line to allow for alignment of the interferometer in the vertical plane.

Optical Considerations

The basic Schupmann medial telescope is shown in Figure 6. Baker [25] describes this instrument in detail. The telescope consists

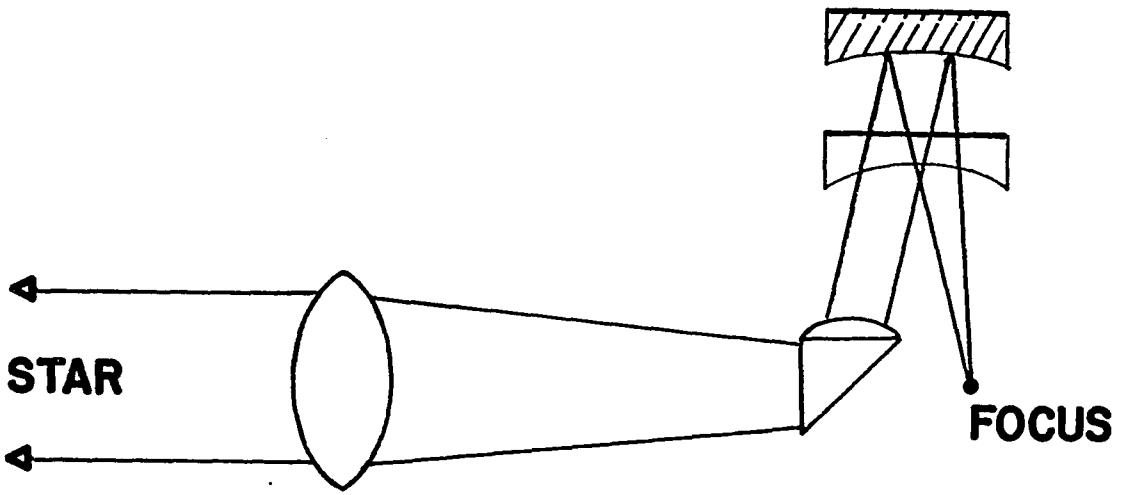

Figure 6. Schupmann telescope.

of a singlet objective, a field lens, and a Mangin mirror. This design has three negative attributes: 1) it does not correct for the lateral chromatic aberration of the atmosphere nor does any other telescope, 2) the field lens must be completely free of imperfections and must be kept completely clean, a result of the field lens being placed at the primary focus, and 3) for zero secondary spectrum, the field lens must be a perfect achromat. A modification of the Schupmann telescope (see Figure 7) results in an instrument which is free of these defects. This telescope reduces lateral atmospheric aberration by a factor of 10^{-2}, has no optical surfaces in the plane of a focus, and reduces the longitudinal chromatic aberration to less than the depth of focus. Light passes through the singlet objective and forms an image at the first focus P_1. The field lens images the objective onto the Mangin mirror and is reflected back through the field lens to the final focus. In actual construction the field lens is two identical lenses at the same longitudinal position laterally offset so that the incoming and outgoing rays pass more nearly through the center of the lens and hence reduce coma. Making two passes through the field lens removes the final image lateral position dependency of field lens position to first order. Using a split field lens adds only the constraint that the halves be fixed in position with respect to each other. Note that there are no optical elements at a focus of the star's image. Thus, small surface imperfections or bubbles cannot cause gross deterioration of the final image.

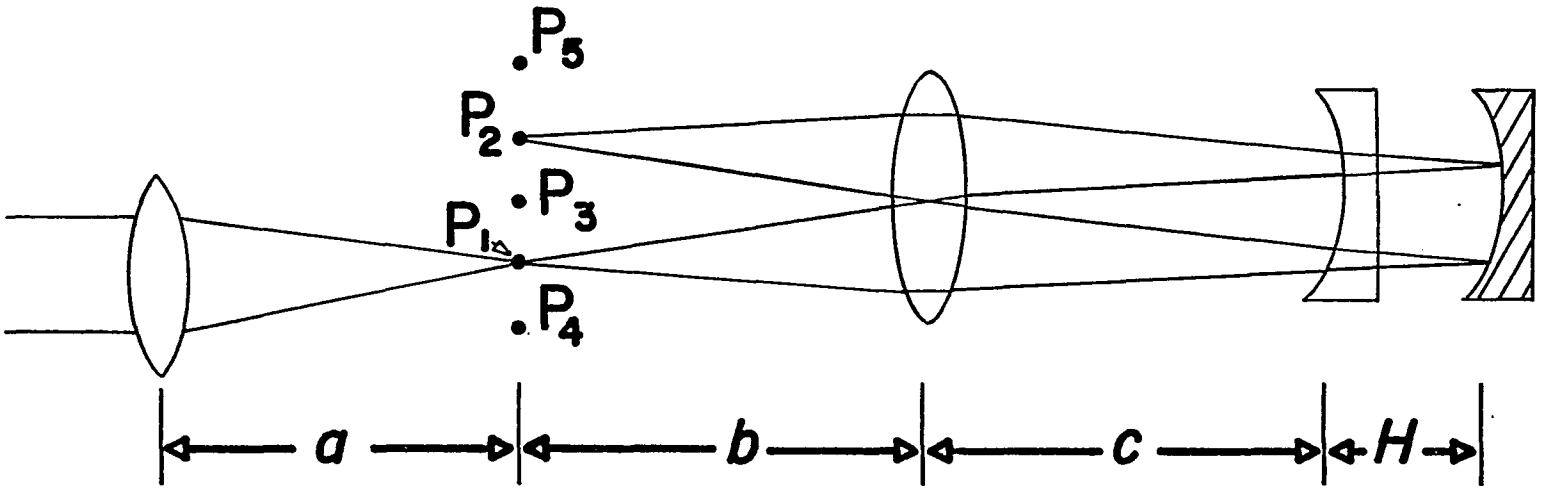

Figure 7. Modified Mangin mirror telescope.

The system constructed has a temperature controlled Invar plate nominally in the plane of the principle focus. The nodal point of the objective to plate distance is fixed to one part in 10^7. This plate has pinholes in it corresponding to P_2, P_4, and P_5 and an aperture for P_1 (see Figure 7). A spring pivot is provided to allow rotation of the Mangin system (Mangin mirror and field lens) about point P_3. The field lens is split, and a carrier mounted in an aluminum tube houses both havles of the field lens. The Mangin mirror is situated at the end of the tube. The Mangin mirror is a plano-concave lens and a concave mirror with an adjustable air gap between them. The mirror itself is mounted on a biomorphic system which allows the mirror normal to be rotated in orthogonal planes. This latter feature is required for angular adjustment of the system and for introducing known motions into the final field so that phase sensitive detection may be performed on the stellar image and the alignment image.

Achromatic Design

Given an objective of Schott BK-7 with a focal length of 1226.3 cm at λ_o = 4861Å, computer-aided design by Hill and Stebbins [26] resulted in a satisfactory set of optical parameters using a singlet field lens displaced from the principle focus. The results are given in Table 5.

A plot of measured final image longitudinal position versus wavelength is shown in Figure 8. The depth of focus of the objective is approximately 1 cm. It is seen that the resultant design has a

Table 5. Telescope optical parameters.

a, b, c, and H are as defined in Figure 7. All lenses are BK-7.

Telescope Optical Parameters	Value in cm
a	1226.3
b	91.44
c	152.4
H	0.923
F.L. of field lens	157.53
F.L. of negative lens	-35.84
F.L. of mirror lens	16.81

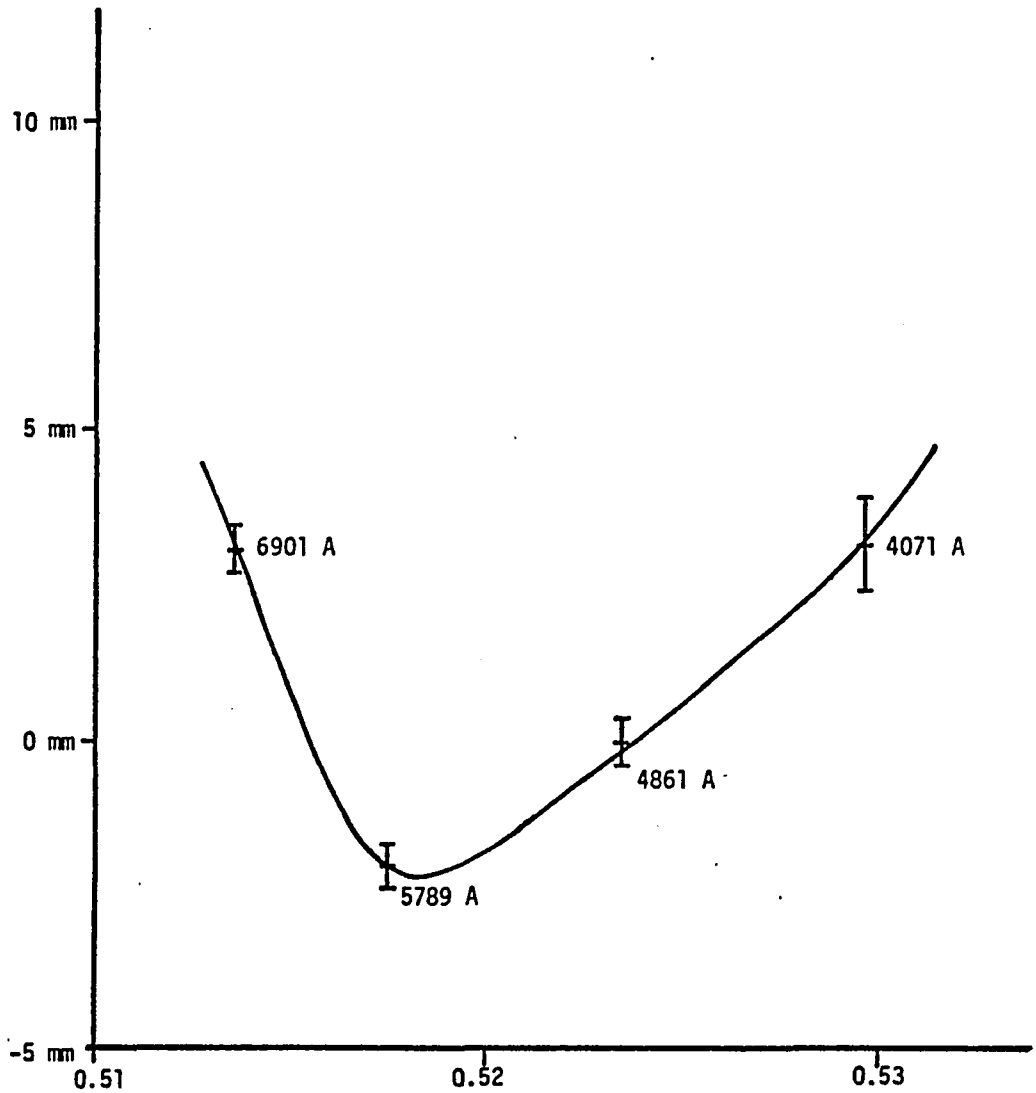

Figure 8. Telescope final longitude focus versus refractivity.

longitudinal chromatic aberration sufficiently smaller than the depth of focus to make further chromatic correction unnecessary.

Longitudinal Alignment of Optical Elements

Given the practical limitations of lens manufacture, it is necessary to have adjustments built into the apparatus to optimize the longitudinal chromatic correction and to focus a system of optical elements which have not been ground to the designed curvatures. Further it is desirable to have these adjustments independent of each other, i.e., one adjustment for correcting the longitudinal position on the final focus at λ_o called q and another adjustment for correcting the dispersion, M. In the Mangin system the two adjustments are the separation of the two elements of the Mangin mirror, h, and the separation of the Mangin mirror and the field lens, c. The following equations give the dependence of $q(\lambda_o)$ and M on c and h:

$$\frac{\partial q(\lambda_o)}{\partial h} = 44 \quad , \tag{51}$$

$$\frac{\partial M}{\partial h} = 28 \quad , \tag{52}$$

$$\frac{\partial q(\lambda_o)}{\partial c} = 0.12 \quad , \tag{53}$$

$$\frac{\partial M}{\partial c} = 2.5 \quad . \tag{54}$$

While c and h are not independent adjustments, the ratio of $[\partial q(\lambda_o)/\partial c]/[\partial M/\partial c]$ to $[\partial q(\lambda_o)/\partial h]/[\partial M/\partial h]$ indicates the following iterative method would be effective in optimizing $q(\lambda_o)$ and c.

Step One: Using light of wavelength λ_o, a point source is placed at P_1 and its conjugate P_2 is found. The position of the focus is determined by occulting the beam with a knife edge while observing it through a low power telescope. The longitudinal position at which the beam is darkened uniformly rather than darkened from one side as the knife edge cuts the beam is the focus. h is adjusted until the longitudinal position is correct.

Step Two: Knowing the dispersion of the objective from calculation or measurement, another point source of light at wavelength λ_1 is placed at the longitudinal position corresponding to this wavelength. Again the position of the conjugate image is found and c is adjusted until the focus of λ_1 light is in the proper position.

Steps one and two are repeated until both colors focus at the correct position. If after step one λ_1 is out of focus by an amount ε_1, step two followed by step one reduces ε_1 by a factor of 0.31. This number is obtained by setting $\delta M = \varepsilon_1$, and circulating through Equations 51 through 54. As a final check, step two measurements without adjustments can be made at several wavelengths to determine how good a fit to the dispersion of the objective one has. In practice, it is found that after the third iteration, the uncertainty in the position of the focus becomes larger than the changes further iterations would make in the focus. M and $q(\lambda_o)$ must be adjusted so that all wavelengths over the usable bandwidth are in focus to within the depth of focus of the objective, 1 cm. Since the alignment observations are made over less than the full bandwidth, measurements to about 0.3 cm are needed to

allow for extrapolation errors. Measurements of this accuracy have been made. Figure 8 shows the degree to which an achromatic fit is achieved.

Lateral Alignment of Optical Elements

Average alignment, i.e., D.C. longitudinal position, of the Mangin is maintained by servoing the image of P_4 onto P_5. In this servo mechanism, P_4 and P_3 are pinholes (0.025 cm dia.). P_4 is illuminated by the objective while the Mangin mirror scans the image of P_4 across P_5. The details of the scanning process are discussed in the following section.

A photomultiplier above P_5 receives the modulated image of P_4 through P_5. Dual frequency phase sensitive detection is performed on this signal and resultant error signals corresponding to the offset of the image of P_4 on P_5 is applied to the angular position transducers which drive the Mangin mirror.

The mechanical arrangement results in a chromatic filter about λ_o, the wavelength which is in focus at point P_4. The chromatic filter property is recognized by observing that some small solid angle of sky $d\Omega$ is mapped into the pinhole opening P_5. P_4 is a pinhole aperture stop situated at the principle focus of the objective for λ_o. The principle focus is not an achromatic focus however. Other wavelengths pass through the pinhole in proportion to the inverse square of their difocused spot size. The wavelength dependence of the transmission T of the filter is given by

$$T(\lambda) = \alpha\left[\frac{\chi(\lambda_o)}{\chi(\lambda)-\chi(\lambda_o)}\right]^2 \tag{55}$$

where $\chi(\lambda_o)$ and $\chi(\lambda)$ are the refractivities of the objective and λ_o and λ respectively.

Using skylight for illuminating P_4 leads to a systematic offset in centering the Mangin mirror. At one solar radius from the limb, the gradient of the intensity divided by the intensity, $(\delta I/dr)/I$, is about $-1.5/R_\odot$ or -1.66×10^{-3}/arc second. The center of the light distribution is found by solving the following equation:

$$\int_{-R}^{C} (R^2-r^2)^{1/2}\ (1 + 1.66 \times 10^{-3} \cdot r)\ dr = \int_{C}^{R} (R^2-r^2)^{1/2}\ (1 + 1.66 \times 10^{-3} \cdot r)\ dr \tag{56}$$

where first term of the integral represents circular geometry of the pinhole and the second term the local intensity plus the gradient. $C = -2.5 \times 10^{-3}$ arc seconds. The sky brightness gradient is determined in the sky brightness servo system to much better than 1%. Calibrating the error signal of this servo system results in a usable means of making the necessary correction to the Mangin align servo to reduce the offset to less than 2.5×10^{-5} arc seconds.

Electronic Components

This section discusses the servo systems and the electronic sampling techniques used in determining a star's position.

Phase Sensitive Detection

There are eight major servo loops used in tracking a star; each one uses a form of phase sensitive detection. A brief outline of phase sensitive detection and how it applies to star detection follows to remind the reader of the important features of this powerful technique. A detector is scanned about a nominal position X_n in the coordinate of the quantity to be measured with a periodic waveform. The center of the stellar flux on the image plane is the quantity to be measured. Scanning with a periodic function $X = X_n + \frac{\beta}{2} \sin \omega t$ generates the time dependent detector signal, $I = R \cdot F(X_n + \frac{\beta}{2} \sin \omega t)$ where R is the detector sensitivity in detector photoelectrons per incident photon. Multiplying this by $\sin \omega t$ and applying a low pass filter gives

$$I_{net}(T) = e^{pt} \int_o^T R \cdot F(X_n + \frac{\beta}{2} \sin \omega t) \sin \omega t \, e^{-pt} \, dt \qquad (57)$$

where p is the time constant of the low pass filter. F(X) may be separated into a light distribution due to a background $F_b(X)$ and that due to the star $F_s(X)$. The first is represented as a power series $F_b(X) = \sum_{n=o}^{\infty} \alpha_n X^n$. It is informative to expand the second component in a Taylor series about the center of the star, X_s,

$$F_s(X) = F(X_s) + F'(X_s) \cdot [X_s + \frac{\beta}{2} \sin \omega t] + \ldots , \qquad (58)$$

$$I_{net} = e^{pt} R \cdot \int_o^T \{ \sum_{M=0}^{\infty} \alpha_M (X_n + \frac{\beta}{2} \sin \omega t)^M + F_s(X_s)$$

$$+ F_s'(X_s) \cdot (X_n + \frac{\beta}{2} \sin \omega t)$$

$$+ \frac{F_s''(X_s)}{2!} [(X_n - X_s)^2 + \frac{\beta}{2}(X_n - X_s) \sin \omega t + \frac{\beta^2}{4} \sin^2 \omega t] \qquad (59)$$

$$+ \frac{F_s'''(X_s)}{3!} [\ldots]^3 + \frac{F_s'^{v}(X_s)}{4!} [X_n - X_s + \frac{\beta}{2} \sin \omega t]^4 + \ldots\}$$

$$\cdot \sin \omega t \, e^{-pt} \, dt \quad .$$

For $T >> \frac{2N\pi}{\omega}$, N large integer, only the even powers of sin ωt survive. This removes $F(X_s)$ and all the even terms in the background sky brightness sum. The most important of the latter sum is of course the dominant M=0 D.C. light level. The odd derivatives of $F_s(X_s)$ are zero because $F_s(X_s)$ is a symmetric function with

$$I_{net} = e^{pt} R \cdot \int_o^T \{\alpha_1 \frac{\beta}{2} \sin \omega t + \alpha_2 \beta X_n \sin \omega t$$

$$+ \alpha_3 (\frac{3}{2} X_n^2 \beta \sin \omega t + (\frac{\beta}{2})^3 \sin^3 \omega t) + \ldots$$

$$+ \frac{F_s''(X_s)}{2!} \beta (X_n - X_s) \sin \omega t \qquad (60)$$

$$+ \frac{F_s'^{v}(X_s)}{4!} [2\beta (X_n - X_s)^3 \sin \omega t + \frac{\beta^3}{2} (X_n - X_s) \sin^3 \omega t]\}$$

$$\cdot \sin \omega t \, e^{-pt} \, dt \quad ,$$

$$I_{net} \propto \alpha_1 \frac{\beta}{4} + \alpha_2 \beta X_n + \frac{3}{4}\beta \alpha_3 [X_n^2 + \frac{\beta^2}{8}] + \ldots + \frac{F_s''}{4} (X_s)\ \beta(X_n - X_s)$$

$$+ \frac{F_s^{IV}(X_s)}{4!} \cdot [\beta(X_n - X_s)^3 + \frac{3\beta^3}{16} (X_n - X_s)] + \ldots \quad . \tag{61}$$

I_{net} is proportional to $(X_n - X_s)$, and hence can be used to servo the center of the detector scan to the point X_s. There are certain restrictions which must be met before a servoed condition can be achieved. $\sum_{M=1}^{\infty} \alpha_M[\ldots]$ must be subtracted from I_{net}. For a small residual contribution of this term a positional offset results. For larger values, I_{net} has no zero. In star detection, a large scan is performed which removes the $\sum_{M=1}^{\infty} \alpha_M[\ldots]$ terms, as discussed later in this chapter in the section on the background sky gradient removal servo.

The $F_s''(X_s)$ must be the dominant term in the Taylor series expansion of the star's image. This is assured if $(X_n - X_s) \cdot \beta$ is sufficiently small. Physically, the positional offset $(X_n - X_s)$ and scan amplitude must be small enough so that the detector sees only the local maximum at X_s. A stellar image has a single maximum; however, large $(X_n - X_s) \cdot \beta$ results in

$$\sum_{j=0}^{\infty} \frac{dF^j(X)}{dX^j} \sim 0 \tag{62}$$

and no servo signal.

Two dimensional phase sensitive detection is performed on the star detector position, Mangin alignment, and lateral color correction servos. Scanning a star distribution in orthogonal directions at different frequencies results in intermodulation. Again a Taylor

series expansion of the vector quantity $F(\hat{Z})$, $\hat{Z} = x\hat{x} + y\hat{y}$, can be used. The previous paragraphs showed that the F"(Z) term is the first contributor to the sum,

$$I_X \propto e^{pt} \int_o^T \frac{F''}{2} (Z_o) (Z-Z_o)^2 \sin \omega_X t + \text{higher order terms} \quad , \tag{63}$$

where I_X is the signal in the X direction integration and ω_X is the scan frequency in the X direction. Separating F(Z) into its components gives

$$I_X \propto e^{pt} \int_o^T \left[\frac{1}{2} \frac{\partial^2 F(X_o,Y_o)}{\partial X^2} (X_n + \frac{\sigma}{2} \sin \omega_X t - X_o)^2 + \frac{1}{2} \frac{\partial^2 F(X_o,Y_o)}{\partial Y^2} (Y_n + \frac{\sigma}{2} \sin \omega_Y t - Y_o)^2 \right] \sin \omega_X t \, e^{-pt} \, dt \quad . \tag{64}$$

The $\frac{\partial^2 F}{\partial x \partial y}$ terms vanish because F is radially symmetric; hence

$$F = F[(x^2+y^2)^{N/2}] \quad , \tag{65}$$

$$I_X = a \frac{\partial^2}{\partial X^2} F(X_o,Y_o) (X_n-X_o) + e^{pt} b \int_o^T \frac{\partial^2}{\partial Y^2} F(X_o,Y_o) \left[(Y_n-Y_o)\sigma \sin \omega_Y t + \frac{\sigma^2}{4} \sin^2 \omega_Y t \right] \cdot \sin \omega_X t \, e^{-pt} \, dt \quad . \tag{66}$$

The first term is the desired servo signal; the integral term is the largest of intermodulation terms, I_{xy}.

$$I_{XY} = e^{pt} \int_o^T \frac{\partial^2}{\partial Y^2} F(X_o,Y_o) \left[\{\cos(\omega_X-\omega_Y)t - \cos(\omega_X+\omega_Y)t\} (Y_n-Y_o)\sigma + \frac{\sigma^2}{4} \{\sin\omega_X t - \frac{1}{2}\sin(\omega_X+2\omega_Y) + \frac{1}{2}\sin(\omega_X-2\omega_Y)t\}\right] e^{-pt}\, dt \quad . \tag{67}$$

For values of $T >> |1/(\omega_X-\omega_Y)|$ and $T >> |1/(\omega_X-2\omega_Y)|$, $I_{xy} \approx 0$. The effect intermodulation has on the experimental design is that it requires the use of scanning frequencies which do not have mutual harmonics.

Online Computer

Each of the star detection servos uses the online computer as an active element. This allows changes in gains and time constants to achieve the optimum configuration for varying conditions, i.e., sky brightness, star magnitude, and seeing. The online computer is also required to furnish calculated rate signals in most servo cases in order to remove velocity errors, and must perform a large number of tasks related to obtaining an invariant solar diameter. All of these tasks are performed in real time and present a considerable load to the computing facility. In order to accomplish all these tasks in real time, the computer data sampling rate or at least the data processing rate must be slow enough to process the initial data before the next data is acquired. Signal-to-noise considerations require a continuous monitoring of detector outputs. Both conditions can be satisfied if

the detector outputs are integrated for the appropriate halves of the detection cycle, then sampled by the computer, at frequencies low enough to satisfy the computer's maximum data rate.

Star Detector Position Servo and Atmospheric Lateral Chromatic Aberration Correction Servo

The star detector position servo, atmospheric lateral chromatic aberration correction servo, and background slope removing servo are an integrated ensemble. Figure 9 shows a functional diagram of this. When switches 1 and 2 are in the A position and lateral chromatic aberration correction loops are closed, the background slopes servo systems are responding to previously acquired data. When switches 1 and 2 are in the B position, the background slope servos are closed and the position and lateral chromatic aberration correction loops are responding to previously acquired data. These switches are computer controlled and the ratio of time in position A to time in position B is determined by requiring the uncertainties in the stellar position due to background slope servo errors to be equal to the uncertainty of the stellar position due to lateral chromatic aberration and positional servo errors.

The star detector position and lateral chromatic aberration correction servo systems are illustrated in terms of their appropriate transfer functions in Figure 10. There are three important features of this servo system. They are: (1) star position and lateral chromatic aberration errors are non-competitive, 2) the star position servos have a rate signal added to the error signal to remove velocity errors, and

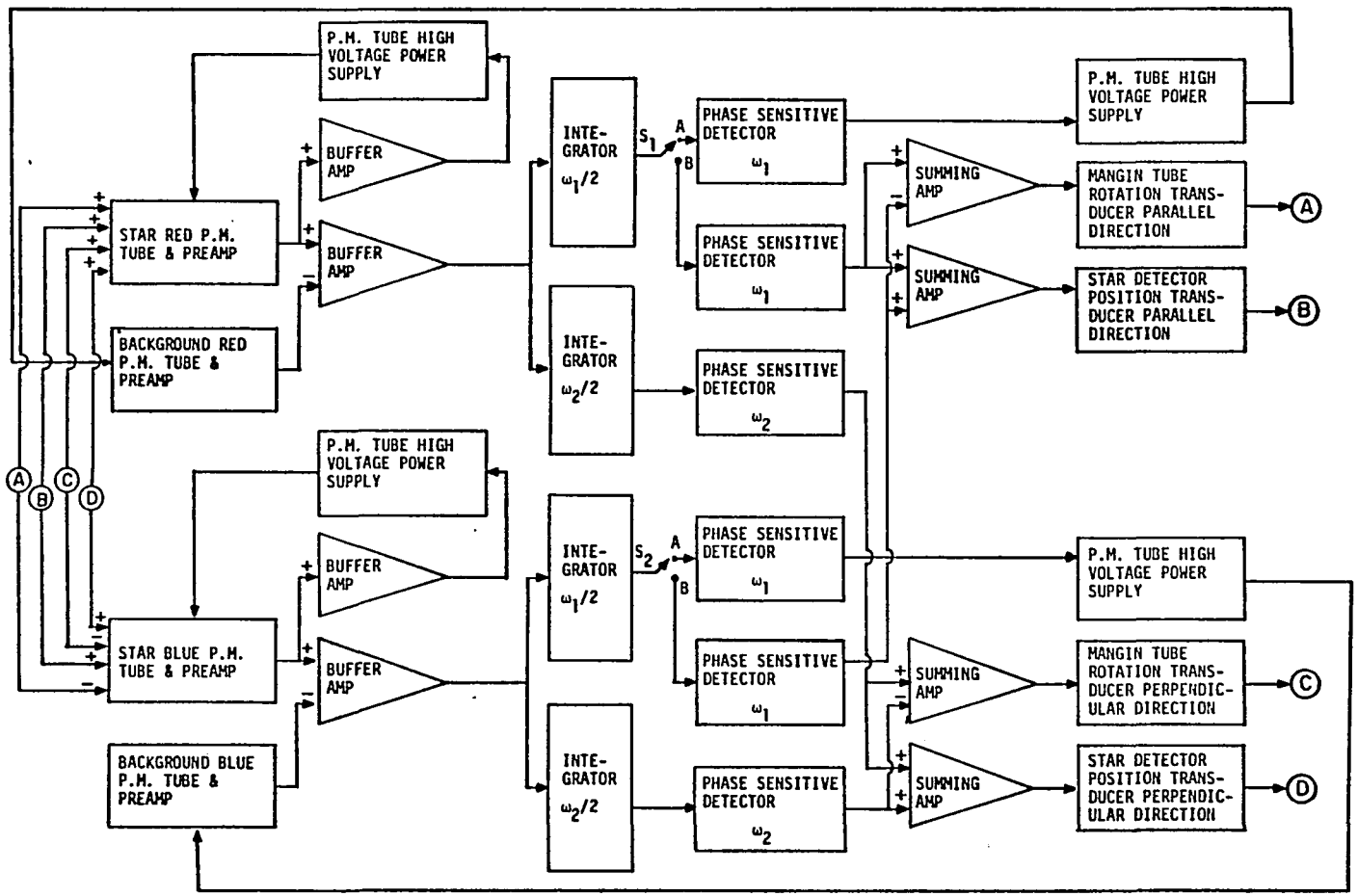

Figure 9. Star detector position servo and atmospheric lateral chromatic aberration correction servo block diagram.

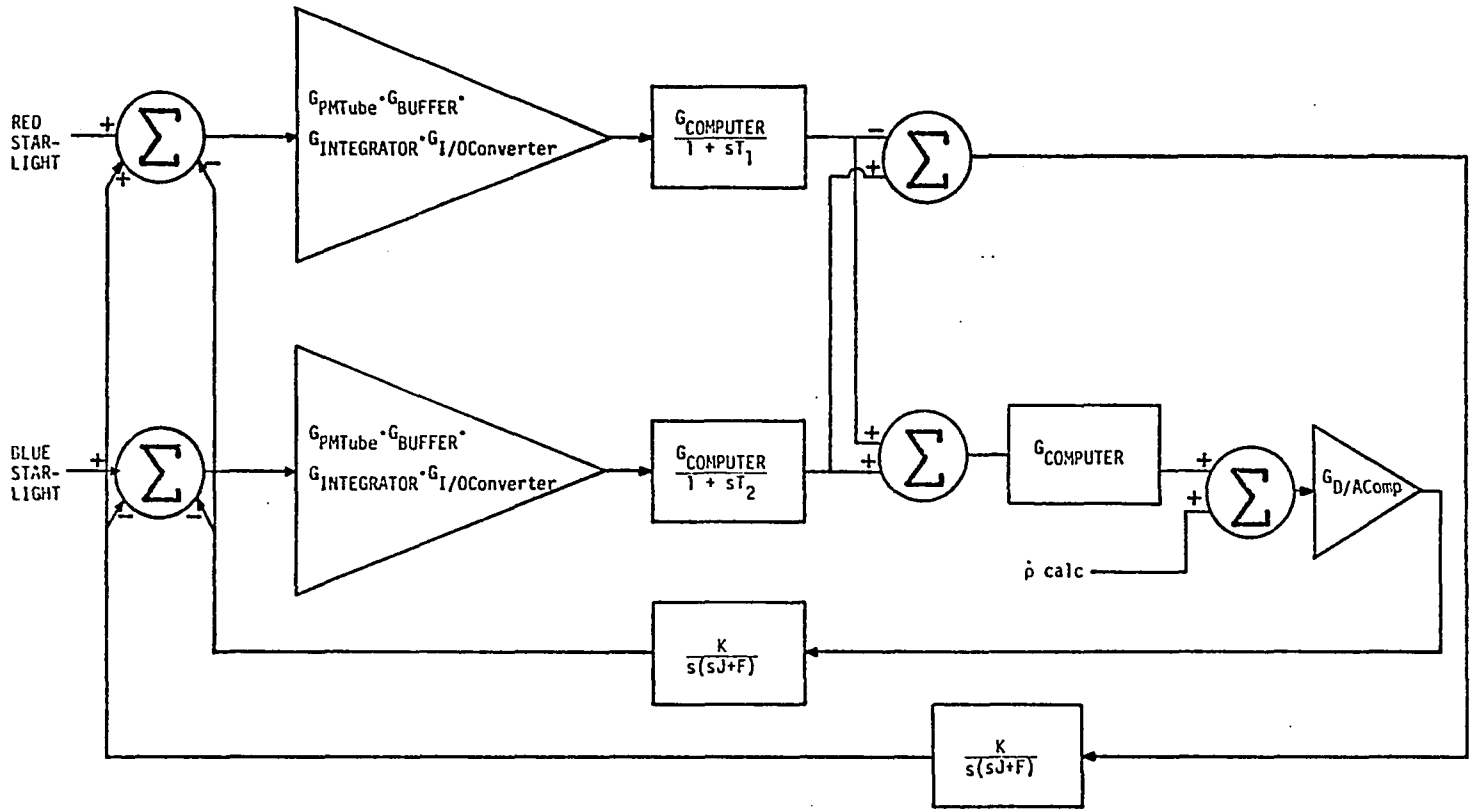

Figure 10. Star detector position servo and atmospheric lateral chromatic aberration correction servo functional diagram.

One direction is shown; the other direction is identical. T = time constant, s = $\delta/\delta t$, G = gain, K = motor torque constant x gear ratio, J = system inertia, F = viscous friction of system.

3) the star position servo uses a rate transducer and a compensating transfer function.

Simultaneous servoing of star position and lateral chromatic aberration removal requires that the error signals be linearly independent. The weighted sum of the red and blue star phase sensitive detectors $\alpha R + \beta B$ is the error signal in the star position servo. Their weighted difference, $\alpha R - \gamma B$ is the lateral chromatic aberration error signal. α, β, and γ are positive coefficients of the same magnitude.

It is necessary to add a calculated star velocity to the error signal to reduce velocity tracking errors. Given a servo system with a gain G and open loop time constant T_1, a velocity V results in a positional error of P, $P = \frac{V \cdot T}{G}$.

In the case of the star detector servo loop, this is

$$P = \frac{0.04 \text{ arc sec/sec} \cdot 1000 \text{ sec}}{1000} = 0.04 \text{ arc sec} . \quad (68)$$

This error is a factor of 40 larger than other systematic errors. Knowing the rate ρ to 10^{-4} reduces the velocity error by 10^{-4} and $P = 0.4 \times 10^{-5}$ arc seconds.

Background Sky Gradient Removal Servo

The background sky gradient removal servo system removes positional errors due to a gradient in the background skylight. This is done by servoing the gain of the background light photomultiplier so that the positional error signal is independent of scan amplitude. In the presence of a background gradient G(x), the star detector position servo controls ϵ so that

$$\int_{-\xi_1+\varepsilon}^{\xi_1+\varepsilon} \{\alpha[S(x) + G(x)] + \beta G(x)\}\, dx = 0 \qquad (69)$$

where ξ_1 is the amplitude of scan in the image field, α and β are real positive coefficients corresponding to the gain of the star detector PMT and amplifier and the background PMT and amplifier. $S(x)$ is an even function representing the stellar light distribution. The additional constraint added by the background sky gradient servo system is

$$\int_{-\xi_2+\varepsilon}^{\xi_2+\varepsilon} \{\alpha[S(x) + G(x)] - \beta G(x)\}\, dx = 0 \qquad (70)$$

where ξ_2 is a scan amplitude, $3\xi_1 \approx \xi_2$, and the parameter servoed is β. The above two equations have a simultaneous solution of $\varepsilon=0$, $\alpha=\beta$. This is the condition of scanning symmetrically about the stellar light distribution and having the background light PMT sensitivity equal to that of the star PMT.

The background sky gradient servo is illustrated in Figure 11, and by transfer function in Figure 12. The star PMT gain is controlled so that the full precision of the A/D may be used. More important, a weak star signal results in a decreased gain which in turn increases the closed loop time constant of the servo system. This reduced closed loop time constant makes the servo system respond more slowly to a weak input signal.

The difference between the star photomultiplier and background photomultiplier signals is integrated over the negative half of a large

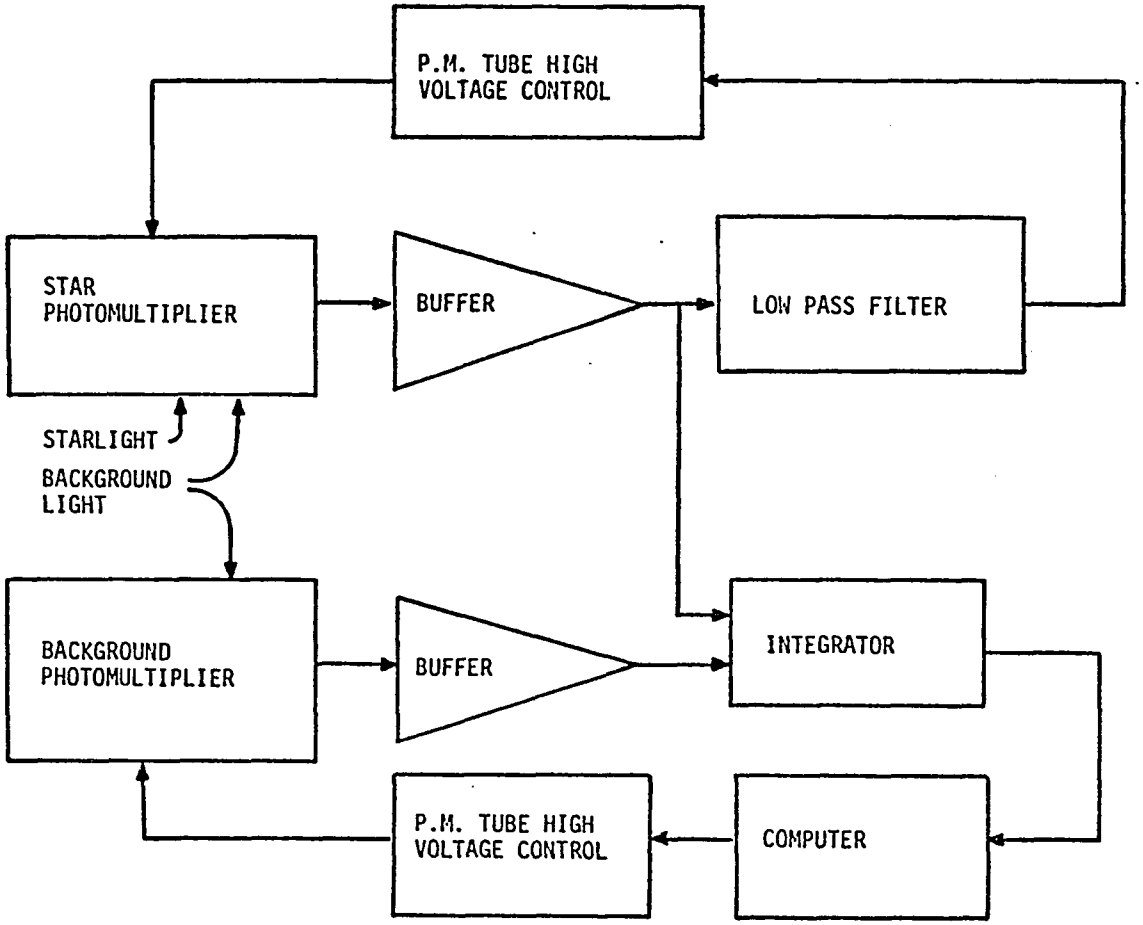

Figure 11. Background sky gradient removal servo block diagram.

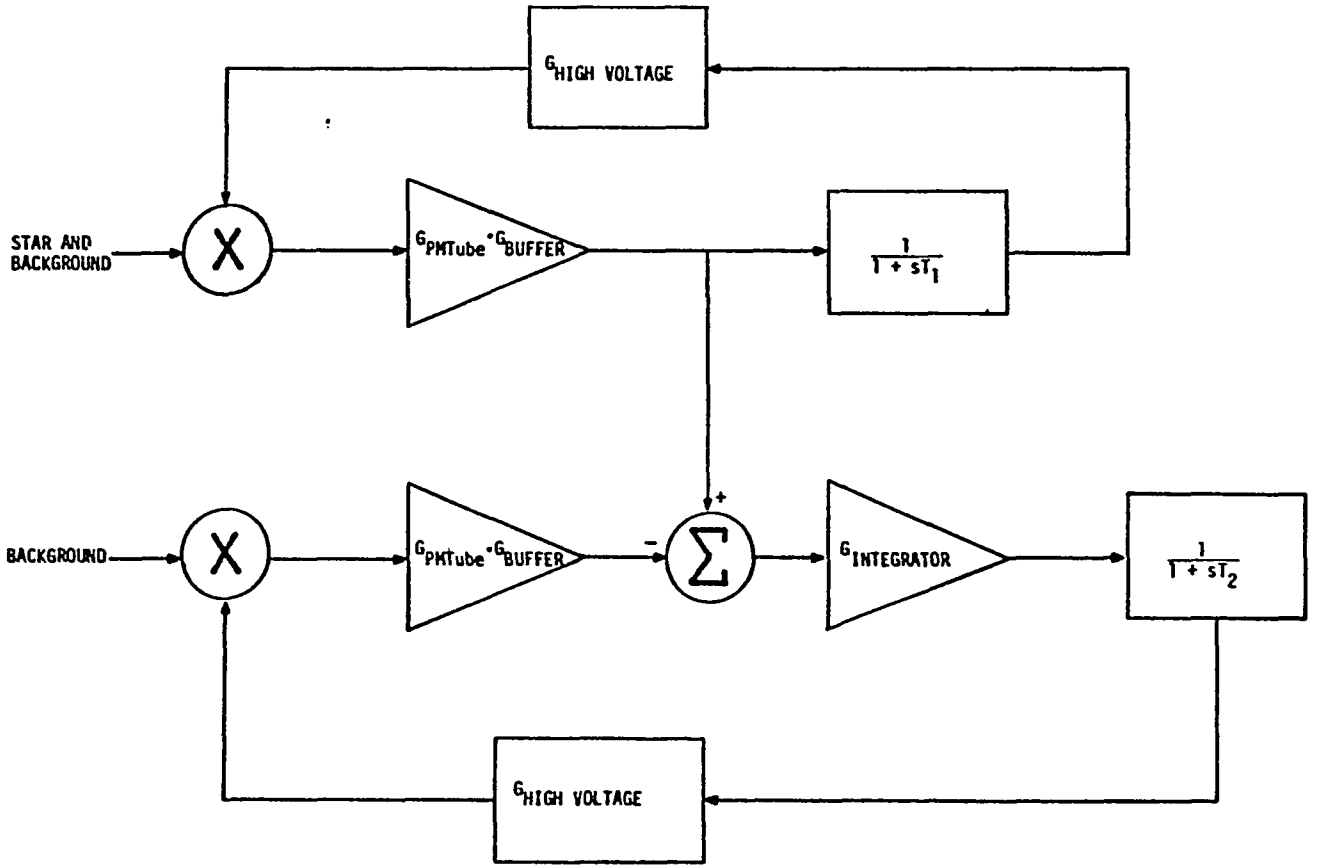

Figure 12. Background sky gradient removal servo functional diagram.

One color is illustrated; both systems are identical.

amplitude scan and is subtracted from the positive half of a large amplitude scan. By large amplitude it is implied that the detector spends most of its time off the image of the star and the gradient signal scales linearly with the scan amplitude. Hence, the majority contribution comes from the background. This signal is suitably filtered and fed into a high voltage controller. As pointed out in Chapter 3, the background slope must be removed to one part in 10^4 if the error due to this is to be less than one millisecond of arc. In the course of tracking a star from $1R_\odot$ to $2R_\odot$, the scattered light is expected to change about a factor of two [22]. In order to accomodate both requirements, the D/A converter must have sufficient precision such that full scale corresponds to a gain of two and the least significant bit represents a change in gain of less than one part in 10^4. A 16 bit D/A accomplishes this. A considerable savings in hardware costs can be had if it is realized that the D/A need not have long term stability nor linearity over its range. All that is required is that it be monotonic over its entire range. The monotonic condition is required to preserve the sign of the error signal with respect to the sign of the gain change. The lack of long term stability is equivalent to gain instability in the background detector system which is being servoed. Hence, this error is self correcting.

Two identical servos are used for background gradient removal, one on the red detector and one on the blue. Since the background gradient is radial to the Sun and this corresponds to the ρ direction, only one dimension is servoed because lengths are being measured only

in the ρ direction. There is essentially no gradient in the direction perpendicular to the solar radius and errors in this direction are a much less serious consideration to the final experimental accuracy.

Mangin Align Servo

The Mangin align servo maintains D.C. alignment of the Mangin mirror. Two noninteracting servo loops are employed, one for the radial direction with respect to the Sun and another for the perpendicular direction. This servo is schematically represented in Figure 13 and functionally represented in Figure 14. These are position servos using position transducers, hence their relative simplicity.

Overall gain of the Mangin align servo system is required to be larger than the open loop offset of the Mangin mirror divided by the ultimate accuracy of the position detector. The operational technique used to satisfy the gain condition is to adjust the mechanical neutral position of the Mangin mirror to that position which results in a minimum error signal in the servo loop. An average open loop offset of one arc second in the Mangin mirror position is typical and a gain of 2000 is sufficient.

Integrator Circuit Design

Certain specific circuits are used throughout the apparatus. While they are not unique, they are not ordinary and are sufficiently important to warrant discussion.

The signals controlling the major servo systems are integrated prior to computer manipulation. The integrator must be resettable by

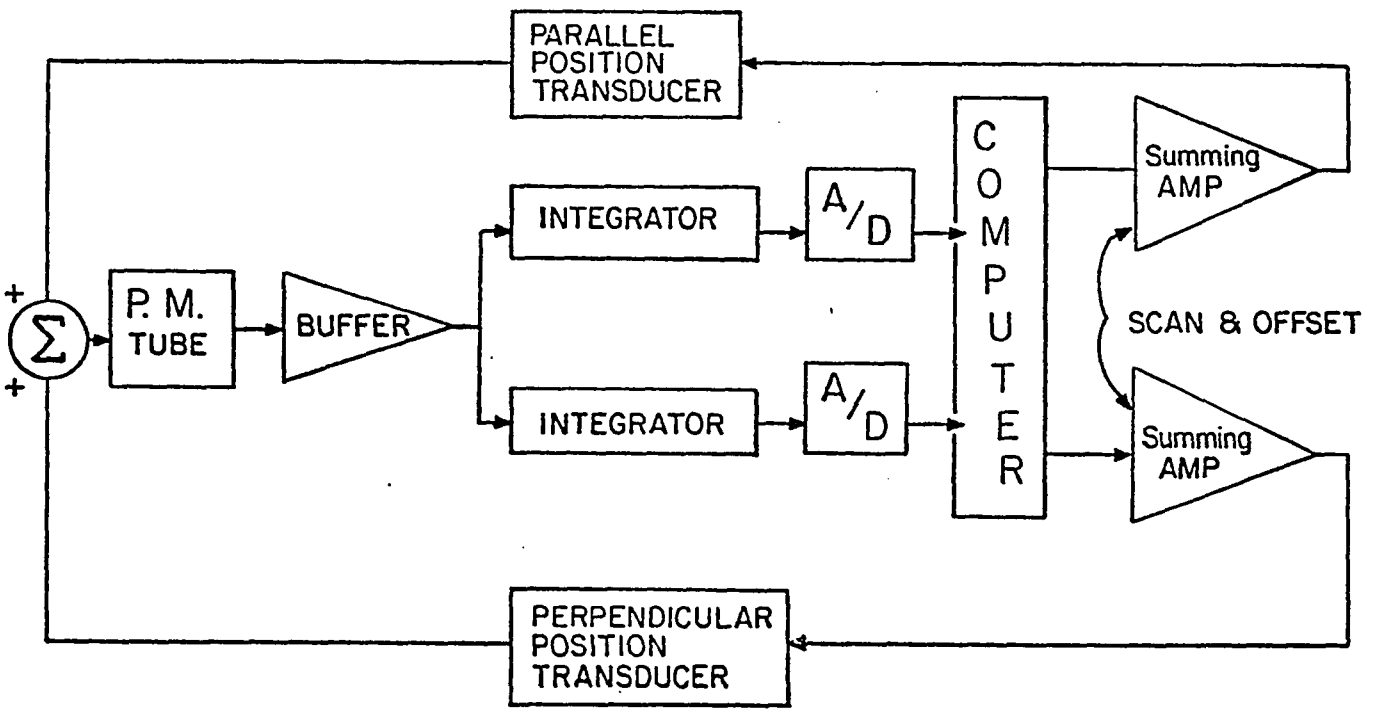

Figure 13. Mangin align servo block diagram.

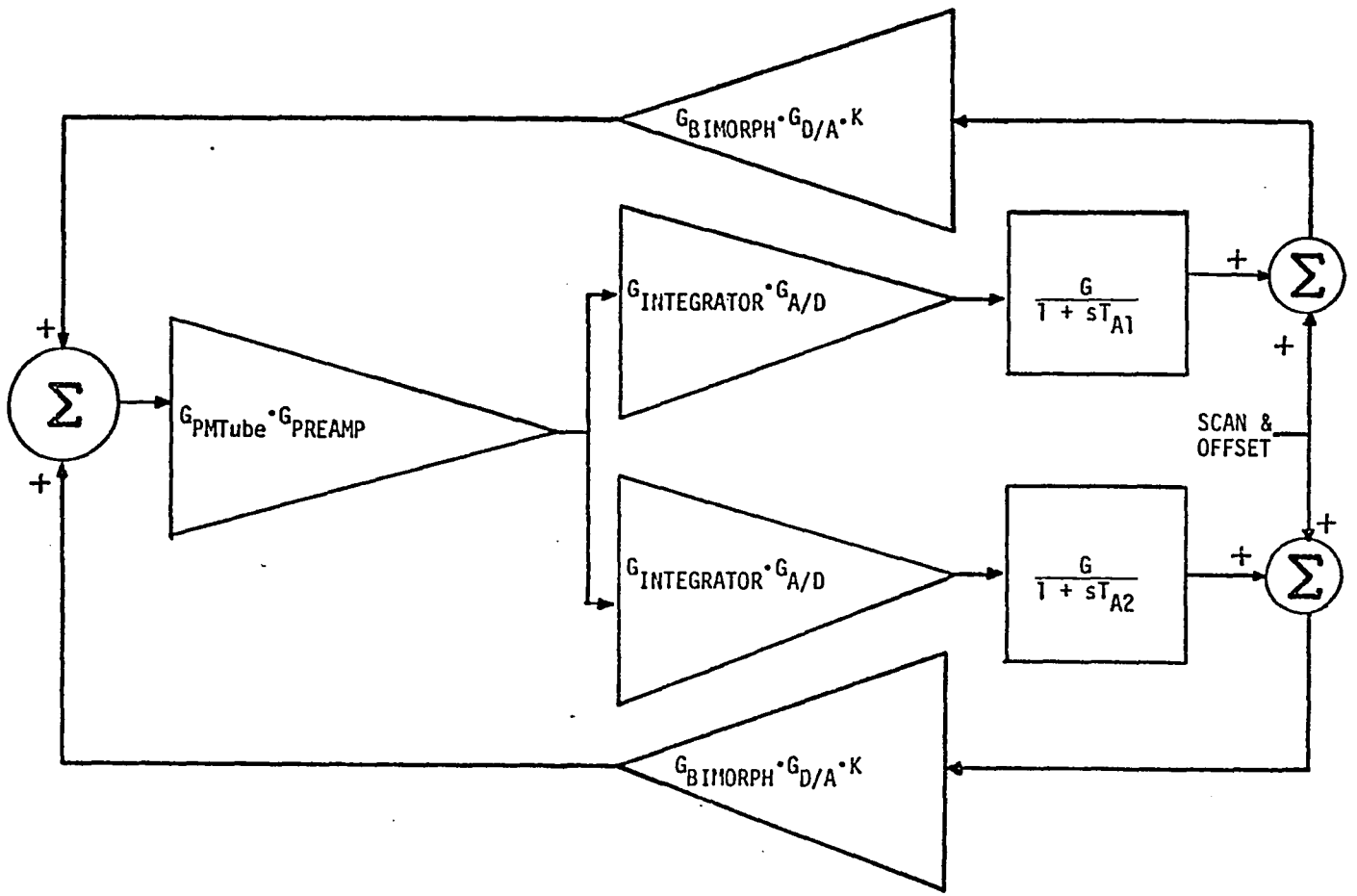

Figure 14. Mangin align servo functional diagram.

K = position to photon conversion constant, s = $\delta/\delta t$, T = integrator time constant.

computer command. Because the integrator is part of an active servo system, it need only treat contiguous half cycles the same. A one part in 10^4 stability between half cycles is required in order that the integrator stability error be less than the ultimate accuracy of the servo system. From a consideration of drift, this amounts to 0.1% per second. The primary source of half cycle to half cycle error is thermal drift in components. The integrating capacitor is the worst problem. A temperature coefficient of 5×10^{-4}/°C is typical of the capacitors used, which insure adequate performance up to unlikely rates of temperature change of 2°C/second.

Figure 15 illustrates the integrator circuit. Synchronizing by computer is effected by momentarily closing a fet switch to establish a unity gain with zero input configuration. The fet "on" resistance is sufficiently low to effectively discharge the integrating capacitor in one millisec. Any residual charge left in the capacitor or any drop in voltage during the integration phase has the effect of changing the weighting factor for various portions of the phase sensitive detection cycle. No displacement of the servoed null occurs for even distributions of starlight.

Computer

The previous section indicated that the servo system contained a computer as part of the loop. The computer has several advantages over hardwired individual systems. Each servo would require a long time constant low pass filter oscillator and a multiplier.

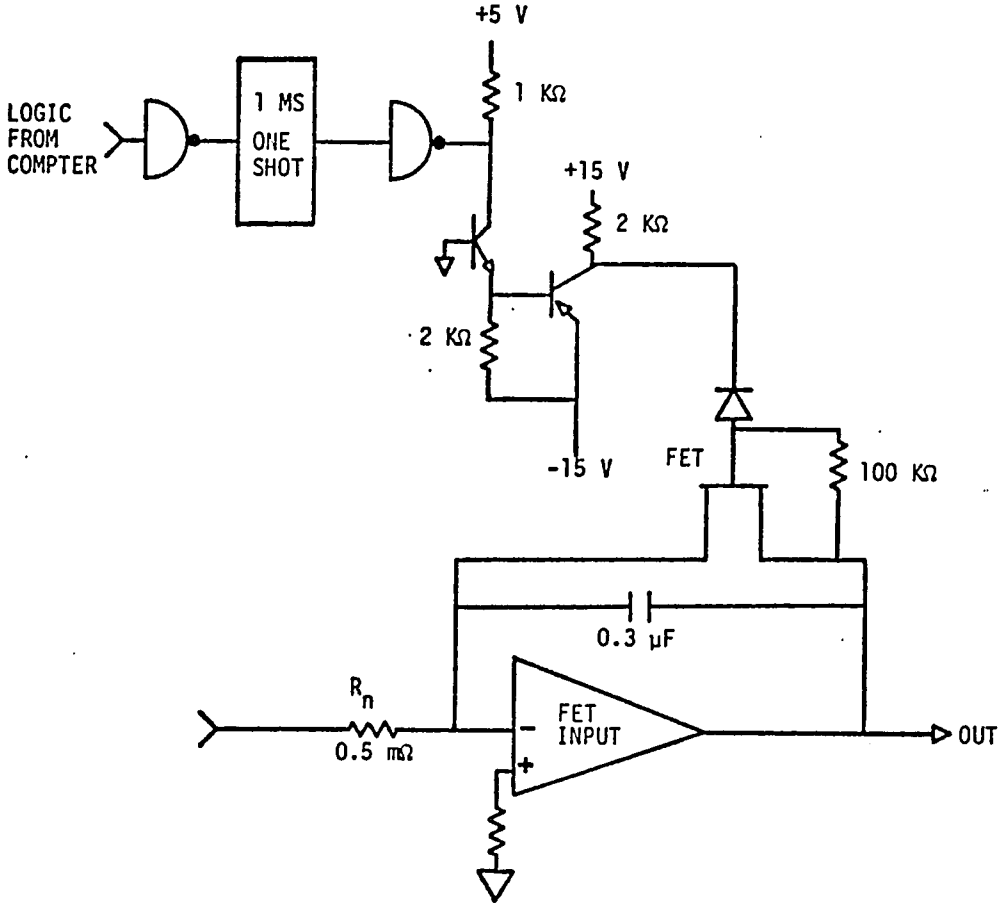

Figure 15. Integrator circuit.

Long time constant, greater than 100 seconds, low pass filters require care in their construction and are subject to noise. The computer can digitally emulate a low pass filter limited only by the A/D and D/A accuracies. Concatanation removes any computer word size limit to filter accuracies. The oscillator function is established by external clocking and internal counters to generate the required low frequencies. A time versus waveform amplitude look-up table for the appropriate waveform can be established. The computer does all these functions in all the servo systems, and is limited only by data processing rate limitations. Having the computer in the loop allows parameters such as gain, time constants, oscillator waveform, and frequency to be easily changed in the software rather than the hardware changes which may be difficult. Another advantage to computer control is the ease and rapidity of overall experimental reconfiguration.

All the star tracking is predicated on having an error signal with which to close the servo loops. Acquisition of a star requires a search of the expected portion of the sky. The star's position and motion are calculated and the star detector is positioned and moved at the proper rate while a search about this moving portion is made.

After the star has been acquired, there is a residual systematic positional error, $\varepsilon = \frac{V\tau}{g}$, due to the motion of the star. Each of the tracking servos has a calculated rate error signal added to offset this error.

Interferometer

The ultimate purpose of accurately positioning a star on a detector is to measure star to Sun distance. This measurement is performed by an interferometer.

The interferometer used for this purpose must be able to maintain its alignment as the star detector and Sun detector are moved relative to each other. The direction of relative motion between the detectors must be determined, and a zero point must be assigned to a specific separation of the detectors. If corner cube retroreflectors are used for the mirrors in an interferometer, the measured mirror to beam splitter distance is invariant under rotations of the corner cube about its apex. The system is also invariant under lateral motion of the corner cube. In tracking the Sun and star, the relative angular orientation and separation of the two detection systems change. The laser light source, beam splitter, reference corner cube reflector, and detector are mounted on the star detector frame and are aligned with the corner cube reflector on the Sun position detector. This alignment is accomplished by servoing the interferometrically measured distance to a minimum using the orientation coordinates of the interferometer as variables.

There are two interferometers used to measure the star-Sun position. A white light interferometer is used to establish a fiducial and a counting interferometer is used to measure distances from the fiducial. This combination of interferometers is discussed by Smolka, Brown, and Hill [27]. The white light interferometer uses a broad band

($\approx$ 500Å) light source and a fringe pattern is observed only when the two arms of the interferometer are very nearly equal. The fiducial is determined by sampling the white light fringes as a function of the laser interferometer counter. This distribution is analyzed by the computer and the counter value corresponding to the fiducial is stored to be used in the data taking procedure.

The interferometer to be used (Figure 16) must be capable of determining the direction and amount of relative motion. The design of this interferometer is the work of Smolka, Brown, and Hill [27] and is thoroughly discussed in their paper. The detector separation is measured to $\lambda/8$. Since measurements will be made over several days over path differences of about 60 cm, a stabilized laser is needed. Temperature stabilization of a low coefficient of thermal expansion laser resonator cavity provides a sufficiently stable light source.

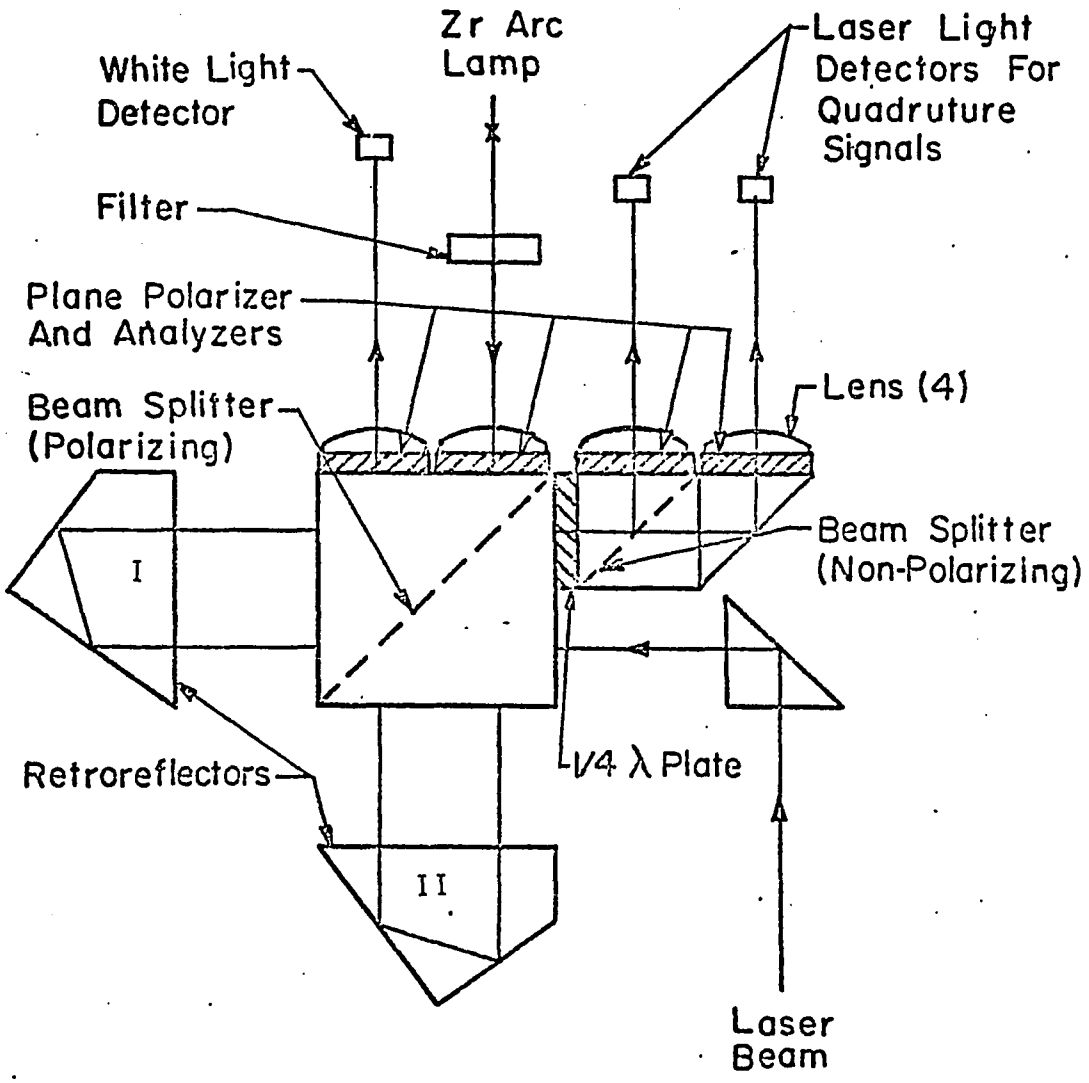

Figure 16. Schematic view of absolute zero reference interferometer. Taken from Smolka, Brown, and Hill [27].

CHAPTER 5

STAR DETECTOR DEMONSTRATION AND CONCLUSION

A portion of the apparatus discussed in the previous chapters has been built and tested. The portion of the telescope required to perform oblateness measurements has been used extensively. The star detector apparatus has been partially built and tested.

The Mangin system has been built and aligned. The longitudinal chromatic aberration of the objective has been corrected by this system. The longitudinal chromation of the system is less than the depth of focus of the objective. The Mangin system has been installed in the telescope and is operational.

The tracking servos have been built and partially tested. Testing the star tracking apparatus was hampered by the fact that the more difficult acquisition portion of the star detection operation must be performed first. The star tracking servos were modified for their initial testing and a manual star acquisition procedure was used. The star position error signals were rerouted to the elevation-azimuth mirrors in lieu of primary tracker error signals. This allows a star to be tracked without the functioning of the Sun primary tracker. A finding telescope was attached to the outside of the elevation cylinder. The star to be tracked was centered in the finding telescope field, then control of the telescope was handed off to an observer viewing the

star's image on the star detector. Orthogonal star position trim signals were made available to the observer who positioned the image of a star over the star detector. With some experience an observer could lock up the servo systems in a few minutes.

Since the observer can see the image of the star only at night, the procedure outlined in the previous paragraph must be used at night. Polaris, visual magnitude 2.4, was the first star to be tracked. Polaris traverses an apparent circle of about 1° radius per day; hence its linear velocity is about ¼° per hour. This is about six times faster than the 1° per day star-Sun relative velocity. Star tracking was performed on January 16, 1974, at 22:45 MST. Polaris was tracked for 55 minutes until a test of servo loop gain forced the star off the tracker. Polaris was reacquired at about 06:30 on January 18, and tracked until 07:32 at which time it was obscured by cirrus clouds. Local sunrise was 07:23. In the one hour tracking time, the photomultiplier dynode chain voltage was reduced from 1060 V to 760 V, reducing servo loop gain by three orders of magnitude.

The SCLERA instrument has demonstrated capability to track stars in the daytime. Much of the additional apparatus required to make meaningful position measurements has been individually tested. Integration of the apparatus into an astrometric instrument capable of the measurements detailed in this dissertation remains an ongoing task.

REFERENCES

[1] von Oppolzer, T. R. Canon of Eclipses. Trans. by O. Gingerich. New York: Dover Publications, Inc., 1962.

[2] Fomalont, E. B., and R. A. Sramek, "A Confirmation of Einstein's General Theory of Relativity by Measuring the Bending of Microwave Radiation in the Gravitational Field of the Sun," Astrophys. J. 199, 749 (1975).

[3] Motz, L., and A. Duveen. Essentials of Astronomy. Belmont, CA: Wadsworth Publishing Co., 1966.

[4] Oleson, J. R., C. A. Zanoni, H. A. Hill, A. W. Healy, P. D. Clayton, and D. L. Patz, "SCLERA: An Astrometric Telescope for Experimental Relativity," Appl. Opt. 13, 206 (1974).

[5] Hill, H. A., and C. A. Zanoni, "Compensation for the Lateral Color Aberration Produced by the Atmosphere," J. Opt. Soc. Amer. 56, 1655 (1966).

[6] Zanoni, C. A., and H. A. Hill, "Reduction of Diffracted Light for Astrometry Near the Sun," J. Opt. Soc. Amer. 55, 1608 (1965).

[7] van Riesbroeck, G., Astron. J. 58, 87 (1953).

[8] Hill, H. A., R. T. Stebbins, and J. R. Oleson, "The Finite Fourier Transform Definition of an Edge on the Solar Disk," Astrophys. J. 200, 484 (1975).

[9] James, J. C., in Radio Astronomy. Ed. by J. V. Evans and T. Hagfors. New York: McGraw-Hill, 1968.

[10] Shapiro, I. I., in Radio Astronomy. Ed. by J. V. Evans and T. Hagfors. New York: McGraw-Hill, 1968.

[11] Shapiro, I. I., G. H. Petlengill, M. E. Ash, R. P. Ingalls, D. B. Campbell, and R. B. Dyce, "Mercury's Perihelion Advance: Determination by Radar," Phys. Rev. Letters 28, 1594 (1972).

[12] Null, G. W., "A Solution for the Sun-Mars Mass Ratio Using Mariner IV Doppler Tracking Data," Astron. J. 72, 1292 (1967).

[13] Duncombe, R. L., "Relativity Effects for the Three Inner Planets," Astron. J. 61, 174 (1956).

[14] Dicke, R. H., and M. Goldenburg, "Solar Oblateness and General Relativity," Phys. Rev. Letters 18, 313 (1967).

[15] Hill, H. A., and R. T. Stebbins, "The Intrinsic Visual Oblateness of the Sun," Astrophys. J. 200, 471 (1975).

[16] N.A.S.A. Factbook. 2nd Edition, Chicago, Illinois: Marquis Academic Media, Marquis Who's Who, Inc., 1975.

[17] Jane's All the World's Aircraft. Ed. by John W. R. Taylor. London: Jane's Yearbooks, 1974.

[18] Anderson, J. L. Principles of Relativity Physics. New York: Academic Press, 1967.

[19] Oke, J. G., "The Hertzsprung-Russel Diagram for F5-K2 Stars with the Most Accurate Absolute Magnitudes," Astrophys. J. 130, 487 (1959).

[20] van Flandern, T. C., Bull. Am. Phys. Soc. 20, 543 (1975).

[21] Stock, J., and G. Keller, in Telescopes. Ed. by G. Kuiper and B. Middlehurst. Chicago, Illinois: The University of Chicago Press, 1960).

[22] Zanoni, C. A., "Development of Daytime Astrometry to Measure the Gravitational Deflection of Light," Ph.D. Dissertation, Princeton University, Princeton, New Jersey, 1966.

[23] Explanatory Supplement to the Astronomical Ephemeris. Ed. by B. L. Garnette and R. V. D. R. Woolley. London: Her Majesty's Stationery Office, 1961.

[24] General Catalogue of 33342 Stars for the Epoch 1950, Carnegie Institution of Washington, D.C., 1948.

[25] Baker, J. G., "The Catadioptric Refractor," Astron. J. 59 74, 1954.

[26] Hill, H. A., and R. T. Stebbins, "SCLERA Progress Report." Department of Physics, University of Arizona, unpublished, 1970.

[27] Smolka, F. M., T. M. Brown, and H. A. Hill, "Corner Cube Interferometer using Extended Sources," Appl. Opt. 15, 2423 (1976).